

**A RICH CLUSTER OF GALAXIES NEAR THE QUASAR B2
1335+28 AT $z=1.1$: COLOR DISTRIBUTION AND
STAR-FORMATION PROPERTIES¹**

Ichi Tanaka, Toru Yamada

Astronomical Institute, Tohoku University, Aoba-ku, Sendai 980-8578, Japan;

ichi,yamada@astr.tohoku.ac.jp

Alfonso Aragón-Salamanca, Tadayuki Kodama

Institute of Astronomy, University of Cambridge, Madingley Road, Cambridge CB3 0HA,

U.K.; aas,kodama@ast.cam.ac.uk

Takamitsu Miyaji

Astrophysikalisches Institut Potsdam, An Der Sternwarte 16, Postdam, Germany

MPE, Postf. 1603, D-85740, Garching, Germany; miyaji@xray.mpe.mpg.de

Kouji Ohta

Department of Astronomy, Faculty of Science, Kyoto University, Sakyo-ku, Kyoto

606-8502, Japan; ohta@kustastro.kyoto-u.ac.jp

Nobuo Arimoto

Institute of Astronomy, University of Tokyo, Mitaka, Tokyo 181-8566, Japan;

arimoto@mtk.ioa.s.u-tokyo.ac.jp

Received _____; accepted _____

¹Partly based on observations made with the University of Hawaii 2.2 m telescope and the Isaac Newton Telescope. The INT is operated on the island of La Palma by the Isaac Newton Group in the Spanish Observatorio del Roque de los Muchachos of the Instituto de Astrofísica de Canarias.

ABSTRACT

We previously reported a significant clustering of red galaxies ($R - K = 3.5-6$) around the radio-loud quasar B2 1335+28 at $z = 1.086$ (Yamada et al. 1997, *Paper I*). In this paper, we establish the existence of a rich cluster at the quasar redshift, and study the properties of the cluster galaxies through further detailed analysis of the photometric data. We also list the positions, K -band magnitudes and colors of all $K < 19$ objects. The near-infrared (NIR) K -band imaging data presented in *Paper I*, together with some additional K -band data, is newly analyzed to study the extent of the clustering of the red galaxies. We also constrain the cluster redshift by applying a robust photometric redshift estimator and find a strong peak around $z = 1.1$.

The color distribution of the galaxies in the cluster is quite broad and the fraction of blue galaxies ($\sim 70\%$) is much larger than in intermediate-redshift clusters. With the help of evolutionary synthesis models, we show that this color distribution can be explained by galaxies with various amounts of star-formation activity mixed with the old stellar populations. Notably, there are about a dozen galaxies which show very red optical-NIR colors but at the same time show significant UV excess with respect to passive-evolution models. They can be interpreted as old early-type galaxies with a small amount (a few % by mass) of star formation. The fact that the UV -excess red galaxies are more abundant than the quiescent red ones suggests that a large fraction of old galaxies in this cluster are still forming stars to some extent. However, a sequence of quiescent red galaxies is clearly identified on the $R - K$ versus K color-magnitude (C-M) diagram. The slope and zero point of their C-M relation appear to be consistent with those expected for the precursors of the C-M relation of present-day cluster ellipticals when observed at $z = 1.1$. The scatter around the C-M line

(~ 0.2 mag in $R - K$) is twice as large as that of the morphologically-selected early-type galaxies observed in rich clusters at $z < 1$, although the uncertainty in the value of the scatter is quite large. We estimate that the Abell richness class of the cluster is $R_{\text{Abell}} \sim 1$. New X-ray data presented here place an upper limit of $L_x < 2 \times 10^{44}$ erg s $^{-1}$ for the cluster luminosity. Finally, we investigate the distribution of the galaxies over larger spatial scales using our optical images, which cover a much larger area than the near-infrared ones. We find evidence that the cluster is located within some lumpy over-dense structures, suggesting that the whole system has not yet relaxed completely and is still dynamically young.

Subject headings: galaxies: elliptical and lenticular, cD — galaxies: clusters: individual (B2 1335+28 cluster) — galaxies: formation — galaxies: evolution — quasars: individual (B2 1335+28) — X-rays: galaxies

1. Introduction

Our knowledge of galaxy evolution in rich clusters at intermediate redshifts ($z \lesssim 1$) has rapidly grown in the recent past thanks both to important observational breakthroughs and the development and improvement of galaxy formation and evolution models. It is now well established that the majority of the early-type galaxies observed in nearby and intermediate-redshift ($z \sim 0.5$) clusters contain mainly old stellar populations formed at high redshifts ($z_{\text{for}} > 2$; e.g. O’Connell 1988; Bower et al. 1992; Aragón-Salamanca et al. 1993; Rakos & Schombert 1995; Gladders et al. 1998; Ellis et al. 1997; Stanford et al. 1998; Kodama et al. 1998).

On the other hand, there is also extensive evidence suggesting that the evolution of the entire cluster galaxy population is not as simple as expected from monolithic formation scenarios. Such evidence is often rather dramatic even at intermediate-redshifts: the fraction of luminous blue galaxies in rich cluster cores is known to increase rapidly with redshift (Butcher & Oemler 1978, 1984; Rakos & Schombert 1995), and spectroscopically ‘active’ (i.e., star-forming) galaxies have been frequently observed in intermediate-redshift clusters (e.g., Dressler & Gunn 1992; Couch & Sharples 1987). Such blue and star-forming galaxies are notably rare in $z \sim 0$ rich clusters. Recent ground-based spectroscopic and *HST* high-resolution imaging observations further revealed a population of old galaxies with on-going or recent (within a few Gyrs prior to the observation) star-formation activity as well as a significantly large fraction of late-type disk galaxies and closely interacting systems (Abraham et al. 1997; Morris et al. 1998; Oemler et al. 1997; Couch et al. 1998; van Dokkum et al. 1998; Poggianti et al. 1999). This ‘active’ evolution of the cluster galaxies is possibly related to the evolution of the morphological mix of the cluster galaxy populations (Dressler et al. 1997; van Dokkum et al. 1998; Kuntschner & Davis 1998).

An important step forward consists of studying clusters at higher redshift, which

can put stronger constraints on both the passive and active evolution of the galaxies. A rapid change in the colors of passively-evolving galaxies only occurs within $\sim 2 - 3$ Gyr after the end of the star formation (e.g., Bower et al. 1992). If cluster early-type galaxies formed at $z > 3$ and evolved passively, one can expect conspicuous color changes only at $z \gtrsim 1$. At the same time, one may expect more frequent star-formation activity at higher redshifts, since there is a significant fraction of galaxies with *post*-starburst signatures in intermediate-redshift clusters (Barger et al. 1996; Postman et al. 1998; Poggianti et al. 1999). A simple extrapolation of the Butcher-Oemler effect (Butcher & Oemler 1984) also predicts a blue galaxy fraction $> 50\%$ at $z \sim 1$. To date, however, only a few rich clusters have been found at $z \gtrsim 1$ and studied in detail with multi-color photometry (Stanford et al. 1997; Yamada et al. 1997), although the number of new candidates is rapidly accumulating (e.g. Postman et al. 1996; Dickinson 1996; Olsen et al. 1998; Hall & Green 1998; Ostrander et al. 1998).

Yamada et al. (1997, hereafter *Paper I*) revealed the existence of a fairly rich cluster at $z \sim 1.1$ near the radio-loud quasar (RLQ) B2 1335+28² through a deep NIR and optical imaging study. The clustering of galaxies in the field was first recognized by Hutchings et al. (1993, hereafter H93). They found a $\sim 3\sigma$ number-density excess of faint galaxies, many of which are blue in $R - I$, and claimed that this region contains a very compact group of starburst galaxies. They also detected 9 emission-line galaxies in the field using a 75Å narrow-band filter centered on the wavelength of the [OII]λ3727Å line shifted to the quasar redshift. In *Paper I*, we showed that the field is characterized by the existence

²In *Paper I*, we used the quasar name Q 1335.8+2834 following H93. But this quasar was first listed in the second B2 catalog of radio sources by Colla et al. (1972). Following the recommendation by the IAU Commission 5 Task Group (chair, H. R. Dickel), we use the original name for this quasar throughout the paper.

of a significant number of very *red* objects in contrast with H93. These red galaxies have optical-NIR colors consistent with those expected for old galaxies at the quasar redshift. Existence of so many red galaxies suggests that they are part of a fairly rich cluster at high redshift, rather than just a group of star-forming galaxies as suggested by H93.

In this paper we present the results of further analysis on this cluster candidate. We add new *K*-band data covering an area to the East of the field previously analyzed in *Paper I*. These data enable us to extend the region of the cluster for which a detailed analysis based on *RIK* photometric data is carried out. At a first glance, galaxies in the cluster region have a very wide color distribution compared to those of nearby and intermediate-redshift clusters, and no clear C-M relation is seen, except for a ‘red finger’ composed of the brightest red galaxies. This may be due to contamination by foreground objects and/or large photometric uncertainties at fainter magnitudes. However, it may also reflect an intrinsic scatter in the stellar populations among the cluster member galaxies such as the presence of different levels of on-going star formation and/or age variations, since these would translate into a significant color scatter. We will show that the latter is the most likely case in our cluster, i.e., the wide color distribution is probably *intrinsic* and can be interpreted as various amounts of star-formation activity in the cluster galaxies.

The paper is set out as follows. Section 2 describes the observations, data reduction, object detection, number counts, and photometry. A catalog of *K*-selected objects is also given. Section 3 describes the spatial extent of the candidate cluster galaxies, and the results of photometric redshift estimates. In section 4 we analyze the optical-NIR colors of the *K*-selected sample. The revised two-color diagram and the C-M diagram are presented. In section 5 we use the *R* & *I* data, which cover wider areas, to investigate the properties of the galaxy clustering on larger spatial scales. Section 6 describes the results of *ROSAT* HRI X-ray observations of the candidate cluster. In section 7, we estimate the cluster richness

and blue galaxy fraction. A brief comparison of our cluster with other high-redshift ones is also given. Section 8 summarizes the main results of this paper.

2. The Optical & Near Infrared Data

Most of the imaging data presented in this paper are the same as those used in *Paper I*, with the addition of a new *K*-band image covering the eastern side of RLQ B2 1335+28. For convenience, we label each region following Figure 1. Since we have already described the data acquisition and reduction procedures in *Paper I*, we only include here a brief description, and add some improvements carried out on the original reduction and analysis. All the data were reduced with the IRAF³ software packages.

2.1. Optical Observations and Data Reduction

The *R*- and *I*-band images were taken with the 1024×1024 TEK CCD camera on the 2.5-m Issac Newton Telescope at the La Palma observatory in February 1995. Total integration times were 8100s for the *R* and 7500s for the *I*-band images. The weather conditions were mostly photometric during the observations, and the seeing conditions were variable, especially during the *I*-band observations. The final co-added images covered an area of 8.8×8.8 arcmin² (900×900 pixel² with a pixel scale of 0.590 arcsec/pixel) and the stellar image sizes were 1.6 and 1.9 arcsec (FWHM) for the *R*- and *I*-band images, respectively.

³The Image Reduction and Analysis Facility (IRAF) is distributed by the National Optical Astronomy Observatories, operated by the Association of Universities for Research in Astronomy, Inc., under contact to the National Science Foundation.

In reducing the optical data, we followed standard CCD reduction procedures. Flat fielding was done using sky-flat frames. The photometric calibration was carried out using standard stars from Landolt (1992) and the magnitudes were converted into the Kron-Cousins photometric system. We neglected the Galactic extinction given the high Galactic latitude of the field ($b = 79.6^\circ$ and $N(H) = 1.1 \times 10^{20} \text{ cm}^{-2}$; Burstein & Heiles 1982; Dickey & Lockman 1990). Zero-point errors are estimated to be smaller than 0.05 mag for the R -band data, but could be as large as 0.1 mag for the I -band data.

2.2. Near-Infrared Observations and Data Reduction

The near-infrared (NIR) images were obtained with the University of Hawaii 2.2-m telescope equipped with the QUIRC camera in February 1996. A standard K -band filter was used. The detector was the 1024×1024 HgCdTe array with a 0.189 arcsec/pixel scale. The F.O.V of the camera is 3.22×3.22 arcmin². In order to make self-flat frames, many dis-registered images with short exposures were taken in a dither pattern of 8-arcsec separation.

We obtained K -band images for the two half-overlapped regions which cover the western and eastern side of RLQ B2 1335+28 (see Figure 2). The western-field frame had a total exposure time of about 6000 sec and was taken under fairly good seeing conditions. We reported the initial results in *Paper I* using this frame (hereafter, *Paper I* frame). The eastern-field frame, however, was taken under poorer conditions and it has two $\sim 100 \times 100$ pixel² -sized ghosts in the area. Only 3450 sec integration was achieved for this frame. We did not use these data (EAST frame) in *Paper I* because of its relatively poorer quality, except when we investigate the spatial distribution of the cluster.

The shapes of the stellar images in the EAST frame are somewhat elongated. We

compensated it by convolution with an ellipsoidal Gaussian kernel. The resulting stellar image-sizes are ~ 2 arcseconds (FWHM). One of the ghost patterns is located in the region which overlaps with the *Paper I* frame, and only the *Paper I* frame is used in the overlapping area. There are only a few sources in the ghost region and it does not affect any statistical results discussed in the following sections. The other ghost image locates at the lower-right (S-W) corner of the EAST frame and we excluded this region in our analysis.

The *Paper I* and the EAST frames are reduced following a similar procedure to that described in Gardner (1995) and are combined after matching the stellar FWHM. As in Figure 1, we refer to their overlapping area as the ‘Cluster’ region, since the galaxy clustering is most clearly seen there. The East and the West sides of the Cluster region are referred to as the ‘Eastern’ region and the ‘Western’ region, respectively.

Magnitude calibration for the *K*-band data is done using three UKIRT standard stars (taken from the on-line lists available at <http://www.jach.hawaii.edu/UKIRT/home.html>). The estimated zero-point uncertainty is ~ 0.04 mag.

Figure 2 shows the *R*, *I*, *K* false-color image of the field. The quasar B2 1335+28 is the blue stellar object shown as ‘QSO’. The F.O.V. of this image corresponds to about 1.5×2.3 Mpc² at the quasar redshift⁴.

2.3. Object Detection and Photometry

For the purpose of our optical-NIR color analysis, we first constructed a catalog of *K*-band-selected objects (to avoid short-term star-formation biases, cf. Aragón-Salamanca et al. 1993) and then searched for their counterparts on the *R*- and *I*-band frames. Object

⁴Throughout this paper, we assume $H_0 = 50 \text{ km sec}^{-1} \text{ Mpc}^{-1}$ and $q_0 = 0.5$.

detection on the K -band frames was carried out using the SExtractor package (Bertin & Arnouts 1996). The detection algorithm uses a $\sigma = 5$ Gaussian kernel and the parameters THRESHOLD= 0.6 & MINAREA= 25 pixel. The MAG_BEST value in the SExtractor output is used as a total magnitude for each object. The Colors are measured in a fixed-diameter aperture of 3.5 arcsec using the IRAF APPHOT package (Davis 1987) after matching the FWHM of each image (FWHM \sim 2 arcsec).

For the faint objects, the photometric errors arise mainly from the sky fitting procedure. We repeated the APPHOT photometry 7 times by changing the radius and width of the sky annulus. By averaging these measurements after excluding the minimum and the maximum values, we obtained the final aperture magnitudes. Since the nominal APPHOT magnitude errors are always smaller than the actual dispersion of the repeated photometry, we used half the range of the magnitudes obtained by this procedure as an indication of the individual photometric error.

2.4. Number Counts

The differential number counts for each frame were used to estimate the detection completeness. Note that the source detection was carried out independently on each frame. Figures 3a and 3b show the results for the R - and I -band data, respectively. Figures 3c and 3d show the K -band counts for the *Paper I* frame and the EAST frame, respectively (see caption).

From Figure 3a & 3b we estimated the nominal detection completeness limit for the R - and the I -band frames to be roughly 25 mag and 23.5 mag, respectively. For the K -band frames, Figure 3c shows that the detection is complete to at least the 19.5 mag bin. The number counts for the Cluster region in Figure 3c and 3d agree very well down to $K = 19$.

Note that the counts for the Cluster region (filled circles) always exceed those of the Eastern region (open circles) in the magnitude ranges $K > 17$, $R = 21 - 23$, and $I = 20 - 23$.

2.5. The Catalog

We present the catalog of the K -band-selected objects with $K < 19$ in Table 1. Column (1) gives the object ID number. The first digit differentiates the region in which each object is located; 1, 2, and 3 correspond to the Cluster region, the Western region, and the Eastern region, respectively. Column (2) & (3) show the coordinates of each object in arcsecs, relative to the quasar position, ie. $(\alpha, \delta) = (13^{\text{h}}38^{\text{m}}07^{\text{s}}.45, 28^{\circ} 05' 10''.7)$; J2000 —Véron-Cetty & Véron 1996). Positive offsets to the west (x) and to the north (y). Column (4) gives the SExtractor MAG_BEST value. The colors $R - I$, $R - K$, and $I - K$ and their uncertainties are shown in Columns (5) – (10).

3. Clustering of Galaxies Near the Quasar B2 1335+28

3.1. Spatial Distribution of the K -Band-Selected Objects

In Figure 4, we show the distribution of all the objects with $K < 19$ detected in the combined K -band frame. Large filled circles, small filled circles, and open circles show the objects with $R - K > 5$, $4 < R - K < 5$ and $R - K < 4$, respectively.

There is strong evidence for the existence of a fairly rich cluster composed of more than 30 red galaxies brighter than $K = 19$. There are only a few red galaxies beyond ~ 20 arcsec East and ~ 80 arcsec West from the quasar. The position of the quasar is offset from the center of the red galaxy clustering.

Although the clustering is stronger for the redder objects, it is also significant for

relatively bluer objects ($R - K < 4$). There are 21 galaxies with $R - K < 4$ and $17 < K < 19$ in the Cluster region while only 8 and 11 in the Eastern and the Western region, respectively, which means that the excess of the galaxies with *blue* opt-NIR color is more than 3σ . The clustering feature seen in our K -selected sample is consistent with that of H93 which reported a clustering of emission-line galaxies and blue (in $R - I$) galaxies in this region (see Figure 4 in H93).

The concentration of galaxies does not look very strong, however, even for the reddest objects. An extended distribution of red galaxies near the south-west edge of the field is also evident. These features may indicate that the cluster is still dynamically young, but the limited sky coverage and lack of radial velocity information prevent us from making a conclusive statement. In section 5, we will come back to this point and discuss it further using the optical data which covers a much wider area on the sky.

3.2. Cluster Redshift and Contamination by Foreground Objects

As we reported in *Paper I*, the optical-NIR colors of the red objects are consistent with those expected for old galaxies observed at $z \sim 1$. The spatial distribution of the emission-line objects in H93 is similar to that of red galaxies, which strongly supports the idea that the detected emission-lines are indeed $[\text{OII}]\lambda 3727$ redshifted to $z = 1.1$ and the cluster is at the redshift of the quasar B2 1335+28.

We have applied a photometric-redshift technique developed by Kodama, Bell, & Bower (1999) to the objects with $K < 19$ in the Cluster region. The code is specially designed to pick up cluster members at high redshift based on an evolutionary population synthesis model. High performance can be achieved when the photometric bands bracket 4000 \AA break, as it is the case here where RIK pass-bands are just catching the break at

$z = 1.1$.

Figure 5 shows the estimated photometric redshifts (solid line) for the $K < 19$ galaxies. As a reference, the observed redshift distribution of field galaxies with $K < 19$ studied by Cowie et al. (1996) is also plotted (dashed line). The strong peak near $z = 1.1$ is prominent. 50 galaxies out of total 105 galaxies are estimated to have the most probable redshift between 0.9 and 1.3. We estimate that the uncertainty in the photometric redshifts could be as large as 0.2 due to the lack of bluer passbands and the relatively large photometric errors (see Kodama et al. 1999). Considering these uncertainties, most of these 50 galaxies are likely to have redshifts near $z = 1.1$. Strong clustering of these objects on the sky, close to the QSO, further supports this view.

From these redshift estimates and the narrow-band data of H93, we conclude that a cluster of galaxy probably exists at $z = 1.1$, although further confirmation by spectroscopic observation is surely desirable.

In fact, the contamination by foreground objects is expected to be small for the reddest objects ($R - K > 5$). Such red colors can be expected only for old galaxies observed at $z \gtrsim 1$. Also, the objects with intermediate colors ($4 < R - K < 5$) are not likely to be foreground galaxies evolving passively at $z = 0.4$ – 0.8 , since they are always too blue in $R - I$ color (see Section 4.2).

For the objects with the bluest colors ($R - K < 4$), the contamination may be larger. For example, some galaxies at $(x, y) \sim (60, -20)$ in Figure 4 are too bright ($K \sim 15$ – 16 mag) to be galaxies at $z = 1.1$. It is possible, however, that except for these bright galaxies, even the galaxies in this color range can be intrinsically blue galaxies at $z = 1.1$. In fact, many of the emission-line galaxies, which are probably at $z = 1.1$, have colors in this range and their clustering properties look similar to that of the red galaxies. In any case, we will need spectroscopic confirmation of these results.

4. Properties of the Cluster Galaxies

4.1. Color-Magnitude Diagram

Figure 6 shows K versus $R - K$ C-M diagram. Filled circles, open circles, and open boxes represent objects in the Cluster region, the Western region, and the Eastern region, respectively. Compared to the C-M diagram presented in *Paper I*, the red sequence of the galaxies at $R - K \sim 5.5$ looks more significant⁵.

However, the distribution of optical-NIR color is relatively broad compared with that of low- and intermediate-redshift clusters. No clear C-M relation can be seen except for a ‘red finger’ seen at $K \sim 17-18$ and $R - K \sim 5.5$. This trend is not so atypical for clusters at high redshifts. Although Stanford et al. (1998) estimated the dispersion of the C-M relation to be as small as 0.1 mag for the *morphologically-selected* early-type galaxies in clusters up to $z \sim 0.9$, the overall color distribution of the entire sample of the cluster galaxies at $z \sim 0.9$ is much broader (see also Aragón-Salamanca et al. 1993). A cluster of galaxies at $z = 1.27$ discovered by Stanford et al. (1997) also has a very broad color distribution except for the ‘red finger’. The color distribution of galaxies in the two clusters at $z \sim 0.9$ studied in Postman et al. (1998) and the 3C 324 cluster at $z \sim 1.2$ in Dickinson (1996) also have similar characteristics.

In Figure 6, we show the color tracks of passively-evolving galaxies using the population synthesis model by Kodama & Arimoto (1997; hereafter KA97). The metallicity-sequence model for early-type galaxies calibrated to the Coma cluster C-M relation (hereafter “Coma C-M model”) is adopted for reference. Thick solid curves show the evolutionary tracks of two model galaxies with different luminosities ($M_V = -22$ and -18.5 mag when they

⁵We found a ~ 0.1 mag calibration error in the K magnitudes reported in *Paper I* due to a software problem.

evolve into $z = 0$) formed at redshift $z_f = 4.4$. The tilted lines connecting the two galaxies mimic the predicted C-M sequence at redshifts $z = 0.2, 0.6, 0.9, 1.1,$ and 1.4 . The tracks for different z_f (2.4 and 1.6) are also plotted.

The observed ‘red envelope’, a sequence of the reddest objects in the C-M diagram, roughly follows the predicted C-M relation for the oldest galaxies ($z_f = 4.4$) seen at $z = 1.1$. Therefore at least some of galaxies in the cluster could be old quiescent galaxies, which are naturally regarded as the progenitor of the very old cluster ellipticals seen in intermediate redshift and present day clusters.

4.2. Two-Color Diagram

In Figure 7 we show the $R - I$ versus $I - K$ diagram for all the objects brighter than $K = 19$ mag. Symbols are the same as in Figure 6 except for the ones enclosed by large diamonds, which indicate the emission-line galaxies from H93. Two large empty diamonds are the emission-line objects with $K > 19$.

The two model tracks show the same Coma C-M model used in the C-M diagrams. The other two tracks labeled as “tau = 1 & 4 model” correspond to continuous star-formation models with exponentially-decaying time scales (τ) of 1 Gyr and 4 Gyr, respectively. We assume that these models mimic the colors of normal disk galaxies; Lilly et al. (1998) showed that the colors of disk-dominated galaxies at $z = 0.65 - 0.87$ are broadly fitted by a similar models with $\tau=5$ Gyr. The formation epoch of the models is set to $z_f = 4.4$, and each track shows the color evolution from $z = 0$ to 1.4 (from blue to red). Tick marks correspond to $\Delta z = 0.1$ intervals. To show the color of galaxies dominated by on-going star-formation at $z = 1.1$, we also consider a model galaxy having a constant star formation rate and the age of 0.5 Gyr (the asterisk labeled as “pure 0.5Gyr burst”). Colors of dwarf

(G0 V – M5 V) and giant (G5 III – M6 III) stars (Johnson 1966; Bessell 1990) are also plotted for reference.

A dozen or so galaxies ($\sim 40\%$ of those with $I - K > 3.5$) have colors consistent with those expected for the passively-evolving galaxies at $z \sim 1.1$. On the other hand, bluer galaxies with $I - K < 3.5$ could be interpreted as continuously star-forming galaxies observed at various redshifts. However, as the excess in surface number density of galaxies in the Cluster region is still higher than 4σ in this color range, we believe that many of them could be blue cluster galaxies at $z \sim 1.1$. Note that many of the emission-line galaxies in H93 also have similarly blue colors.

There are also red ($I - K > 3.5$) galaxies which are bluer in $R - I$ than the passively-evolving galaxies ($R - I < 1.3$). Their $R - I$ and $I - K$ colors cannot be reproduced either by passively-evolving galaxies or by mildly evolving, continuously star-forming galaxies at any redshift. The $I - K$ colors are too red for continuously star-forming models with $\tau > 1$ Gyr for any given $R - I$ color; their NIR light must be dominated by old stars and some amount of UV excess is needed to explain their observed blue $R - I$ colors. Hereafter we refer this population ($I - K \gtrsim 3.5$ and $R - I \lesssim 1.3$) as ‘ UV -excess red galaxies’.

On the whole, the galaxies in the Cluster region constitute a broad sequence from the ‘Coma C-M model’ to the ‘recent 0.5 Gyr burst model’. We try to explain this sequence by adding different amounts of a star-formation component to the old passively-evolving galaxy model at $z = 1.1$ (hereafter we will call the former the SF component and the latter the OLD component). The rest frame near- UV color ($\sim R - I$ color at $z \sim 1.1$) of the model galaxy is determined by the ratio between the SF component (star-formation rate) and the OLD component. As a template spectrum of the SF component, we adopt a constant-SFR model with solar metallicity, Salpeter IMF (mass cutoffs $M_l = 0.1 M_\odot$ and $M_u = 60 M_\odot$), observed 0.5 Gyr after the onset of star formation. These $OLD+SF$

models can also mimic the colors of exponentially-decaying models observed at $z = 1.1$. For convenience in characterizing the amount of the SF component relative to the OLD one, we introduce the burst strength, f_{burst} , which is defined here as

$$f_{\text{burst}} = \frac{SFR \cdot t_{\text{burst}}}{M_s} \quad (1)$$

The f_{burst} value represents the mass fraction of the burst population to the total stellar mass M_s (i.e., SF and OLD component). Note that this value depends on the duration of the burst, t_{burst} , which is arbitrary chosen to be $t_{\text{burst}} = 0.5$ Gyr here. However, the location of the model tracks on the two-color diagram does not change significantly when varying t_{burst} .

The results are shown in Figure 8. Many galaxies in the Cluster region seem to follow the model track⁶ from a pure passively-evolving galaxy to a pure star-burst one. Thus, the broad color distribution of the galaxies in the Cluster region can be explained by the variation of the fraction of the SF component in galaxies at observed at $z = 1.1$.

Many of the emission-line galaxies detected by H93 lie around the track of large burst strengths, supporting the hypothesis that the emission line is indeed the redshifted [OII] $\lambda 3727\text{\AA}$ from the star-forming galaxies in a cluster at $z \sim 1.1$ (Kennicutt 1992). The [OII] emission-line flux may affect the I -band flux of objects at $z = 1.1$. We show the effect of an emission line with equivalent width (EW) of 100\AA by an arrow on the bottom right-hand corner of Figure 7. The effect of reddening is also shown, using the extinction curve of Savage and Mathis (1979). An emission line with an EW of 100\AA is probably too extreme, judging from Figure 2 in H93. However, an extinction of $A_V = 0.5\text{--}1$ mag may well be present in star-forming galaxies at $z > 1$ (e.g., Glazebrook et al. 1998; Sawicki &

⁶The photometric redshift measurements presented in Section 3 are just another representation of this fact; see Kodama et al. (1999).

Yee 1998).

Two red [OII] emission-line galaxies locate just on the color track of the passive-evolution model at $z \sim 1$. According to H93, both have $\text{EW}([\text{OII}]) \sim 50\text{\AA}$. Considering that there is no sign of star formation in their colors, these emission-lines may originate from AGN activity. In fact, Dressler et al. (1985) found that some galaxies have strong [OII] emission and red colors in clusters at $z < 0.5$, all of them identified as AGN (Dressler, Thompsom & Schectman 1985; Kennicutt 1992).

The UV -excess red galaxies lie at $f_{\text{burst}} \lesssim 0.03$, and the amount of SF component required to explain the excess UV light seems to be small. It is worth noting that the fraction of such object is very large in this cluster. Among galaxies with $19 < K$ and $I - K > 3.5$, more than 60% show the UV excess. Although Smail et al. (1998) have shown that a similar kind of UV -excess galaxies exist in clusters at $z \sim 0.2$, the fraction is comparatively small (at most a few %).

There are several possible interpretations for the relatively large abundance of these UV -excess red galaxies. If the star-formation events occur intermittently in each individual galaxy (triggered, perhaps, by infall of small gas clouds and/or gas-rich galaxies, or regulated by some internal process such as refueling by stellar mass-loss), those events must be very frequent. The time interval for such events must be comparable with the duration of each star-formation episode. Another possibility is that the majority of the galaxies in the cluster are still at the last stages of their formation. Their colors may be explained by exponential models with τ smaller than 1 Gyr. The star-formation time scale for these galaxies may be short but the star-formation tail may be still significant.

The UV -excess red galaxies may be related to the galaxies with larger f_{burst} in a time sequence. Since strongly star-forming galaxies are much rarer than quiescent early-types in low- to intermediate-redshift clusters, the galaxies with large f_{burst} have to disappear by the

present epoch. While they gradually cease their star formation and turn into red quiescent galaxies, they may pass through the *UV*-excess red (small f_{burst}) phase.

It is worth considering the possible relationship between this on-going star-formation activity in cluster galaxies at $z \sim 1.1$ and the *post-starburst* features seen in many galaxies in clusters at lower redshift. Spectroscopic studies have revealed the existence of a significant fraction of post-starburst galaxies in clusters at $z = 0.3 - 0.5$ (e.g., Dressler & Gunn 1992; Couch et al. 1994, 1998; Poggianti et al. 1999). These post-sturburst galaxies must have experienced some star formation at higher redshifts. The weak fossils of the past star-formation activity seen as relatively-strong Balmer absorption lines in the spectra of the intermediate-redshift cluster galaxies can be seen only during \sim a few Gyr after the star-formation episode ceased. It is thus not surprising that we see a large fraction of star-forming galaxies instead of post-starburst galaxies in high-redshift clusters at $z > 0.5$. The observed large fraction of star-forming galaxies in the cluster near B2 1335+28 may imply that such star-formation events are already active at $z \sim 1.1$. Postman et al. (1998) also found another example of a cluster at $z = 0.9$ with a large fraction of star-forming galaxies.

4.3. Identifying the Color-Magnitude Sequence of the Cluster at $z=1.1$

Our revised C-M diagram (Figure 6) shows only a broad distribution of red galaxies but not a tight C-M relation. As seen in the last subsection, the main reason for this wide distribution of colors is likely to be the on-going star-formation events with various strengths. Here we attempt to exclude galaxies having star formation to retrieve a C-M sequence made of quiescent galaxies.

From the model calculation shown in Figure 8, we see that the effect of star formation

is to make the $R - I$ color bluer while the age and metallicity differences do not affect this color so much. As seen in Figure 8, the passive evolution track at $z \sim 1.1$ predicts $R - I$ colors redder than 1.3. By selecting galaxies with $R - I > 1.3$, we can thus effectively reject star-forming objects while this introduces little bias for objects of various ages or metallicities. In other words, with this criteria we can exclude the objects which have UV excess with respect to the expected spectrum of passively-evolving galaxies.

Figure 9 shows the results (9a for $R - K$ versus K and 9b for $I - K$ versus K). Objects with $R - I > 1.3$ are marked by symbols with a small dot (hereafter we refer to them as the *quiescent members*). The dashed line shows the C-M relation at $z = 1.1$ predicted by the Coma C-M model with $z_f = 4.4$.

A fairly well defined C-M sequence appears in Figure 9. It seems to follow the expected C-M relation at $z \sim 1.1$ about ~ 3 magnitude range and it is compatibly with being the precursor of the C-M relation seen in low-redshift clusters. We applied a least square fitting algorithm with 2-sigma rejection clipping (three outlying galaxies are rejected) for Figure 9a and obtained a best-fitting slope of -0.01 ± 0.1 . We also estimated the r.m.s. scatter using the biweight scale estimator after 2-sigma rejection clipping (Beers, Flynn, & Gebhard 1990). The resulting scatter is found to be $0.22_{-0.03}^{+0.05}$ for $R - K$, which is significantly larger than the photometric uncertainties. This scatter is about a factor of two larger than that found for the morphologically-selected early-type galaxies in a cluster at $z = 0.895$ observed by Stanford et al. (1998).

There could be several causes for this relatively large scatter under the assumption that the sequence defined by the *quiescent members* is really a precursor of the C-M relation at lower redshifts. Some small amount of star formation can remain, but the effect is likely to be small, since the galaxies with significant star formation were excluded with our $R - I$ selection cutoff. Another possibility is a chance projection of two poorer clusters

with $\Delta z \sim 0.1$. This possibility cannot be excluded without spectroscopic redshifts. And a certain amount of spread in the ages of the *quiescent members* remains an interesting possibility. We can evaluate the age spread needed to explain the scatter by comparing the observed colors with the models. Note that the following arguments are sensitive to the true cluster redshift and/or to systematic zero-point errors in our photometry. Independent photometry and spectroscopic redshift measurement are needed before obtaining more reliable values.

In Figure 9, we show the colors of passive evolution models with various ages at the observed redshift. Thick lines are for a metal-rich, bright galaxy model ($M_V = -22$ or $K \sim 17$ mag) and thin lines for a metal-poor, faint one ($M_V = -18.5$ or $K \sim 21$ mag). Comparing with the observed colors, we see that the mean stellar age of the passively-evolving galaxies in the cluster seems to spread over a ~ 1 Gyr range. This amount of age spread does not conflict with the tight C-M relations observed in clusters at $z \lesssim 0.5$. As shown in Figure 6, even the models with an age difference of 2 Gyr at $z = 1.1$ rapidly evolve and become indistinguishable at $z = 0.6$. The major star-formation epoch in these *quiescent members* is likely to be $z_f = 2-5$ and possibly not before $z_f \sim 5$ with the adopted cosmology.

5. Spatial Distribution of the Optically-Selected Sample

In this section we analyze the spatial distribution of galaxies selected from the optical CCD (R & I) data. The CCD frames cover a wider area on the sky (five times larger) than the K -band frames. As the clustering of red galaxies seems to extend beyond K -band frames (Section 3.1), the inspection of the galaxy distribution on larger scales is necessary to constrain the whole extent of the cluster.

We extract cluster galaxy candidates in a somewhat *a posteriori* manner, using the information obtained in the previous discussion. We choose galaxies with $R - I$ colors and I magnitudes similar to those of the *red* candidate cluster members found in the K -selected sample. Although some contamination by foreground galaxies and the drop out of some bluer cluster galaxies are inevitable, this procedure is likely to maximize the contrast of the putative cluster galaxies over the field galaxies.

In Figure 8 we see that many galaxies in the Cluster region have colors $R - I > 0.8$ while few galaxies in the Western and the Eastern regions locate in this color range. Passively-evolving old galaxies at $z = 1.1$ have colors $R - I > 1.3$. The brightest [OII] emitter satisfying the red color criteria has $I = 21.1$ mag. Thus, we select the objects which have colors and magnitudes $21 < I < 23.5$ and $R - I > 0.8$ for the cluster galaxy candidates and especially those with $R - I > 1.3$ for candidates of passively-evolving galaxies in the cluster. The limit of $I = 23.5$ is chosen for reliable color measurements.

We plot the sky distribution of all galaxies with $I < 23.5$ in Figure 10. The red objects with $21 < I < 23.5$ are marked by the filled circles. We can see that the red galaxies (large filled circles for $R - I > 1.3$ and small filled circles for $0.8 < R - I < 1.3$) are clearly clustered around the coordinates $(0, -50)$. There seems to be other significant excess features near $(100, -100)$ and $(180, -100)$. Since a part of this ‘southern extension’ of the cluster is also seen in the distribution of the K -selected galaxies and some of them have red optical-NIR colors consistent with galaxies at $z = 1.1$, we speculate that these features are related and possibly connected with each other in real space. Thus, the whole red galaxy clustering seems to extend beyond the K -band area in the South-West direction and it may be a fairly elongated structure. There is another concentration of faint red galaxies around $(0, 250)$, far North from the quasar B2 1335+28; H93 also comments on a slight galaxy excess North of the quasar.

6. The *ROSAT* HRI Observation and Results

With the aim of investigating the possible extended X-ray emission associated with the cluster, we have observed this field with the *ROSAT* High Resolution Imager (HRI, David et al. 1996). A 44.0 ks exposure centered on $(\alpha, \delta) = (13^{\text{h}} 38^{\text{m}} 31^{\text{s}}.0, 28^{\circ} 06' 00'')$ (J2000) was made with B2 1335+28 located in the central region of the FOV (off-axis angle = $5'.3$). In our analysis, we have only used the HRI raw pulse height channels between 2 and 8, where the loss of the cosmic signal is minimal ($\sim 7\%$) and at the same time the particle background can be significantly reduced (David et al. 1996). We have also excluded the time intervals where the remaining background level is high. A 35.6 ks total exposure remained after screening.

A faint point-like X-ray source was clearly seen at the position of the quasar B2 1335+28 itself on the screened image, but no evidence for extension of this source was present. We have further searched for extended X-ray emission which might be associated with the cluster. A total of 271 HRI counts were present within the $1'$ (~ 0.5 Mpc) radius region centered on the G1 galaxy, excluding the $10''$ radius region around the quasar. The background count estimated from the surrounding annular region ($1'-5'$), scaled by area, was 274. The $1'$ region centered on the center of light of the red galaxies ($R - K > 4$) contained 276 HRI counts, while the scaled background count was 268. In either case, no significant X-ray enhancement was found.

These numbers lead to a 3σ upper-limit to the HRI count-rate in the 1 arcminute-radius region of 1.4×10^{-3} cts s^{-1} . This upper-limit count-rate corresponds to a 0.5–2 keV luminosity of 2×10^{44} erg s^{-1} , assuming Raymond & Smith plasma spectra (distributed as a part of XSPEC; Arnaud 1996) with plasma temperatures appropriate for a galaxy cluster ($2 \lesssim kT \text{ keV} \lesssim 8$) and chemical abundance of 0.3 (solar), placed at $z = 1.1$, and absorbed by our galaxy ($N_{\text{H}} = 1.1 \times 10^{20}$ cm $^{-2}$; Burstein & Heiles 1982; Dicky & Lockman 1990).

The implications of this upper-limit luminosity are discussed in the next section.

7. Discussion: Cluster Properties

7.1. Cluster Richness

We will estimate the cluster richness from both the K -selected data and the optical CCD data. The most popular method to determine the cluster richness is that defined by Abell (1958). Abell cluster richness (R_{Abell}) is the number of cluster galaxies within an area of 1.5 Mpc radius and in the magnitude range $m_3 - m_3 + 2$ (m_i is the magnitude of the i -th brightest galaxy in a cluster). However, these values are easily affected by the evolutionary properties of the cluster galaxies and by the assumed cosmology when the clusters are at high redshift. The uncertainty in the field correction also becomes rather large at $z > 1$. Therefore the richness values obtained here should be regarded as an indicative.

First, we estimate the richness using the K -selected sample. The third brightest galaxy among the *red* ($R - K > 5$) ones has $K \sim 17.2$ mag. There are 69 galaxies in the Cluster region in the magnitude range between 17.2 and 19.2 mag and 15 and 19 galaxies in the Eastern and the Western region, respectively. The net galaxy excess of the Cluster region thus contains ~ 50 galaxies, although this may be an underestimate since the Eastern and the Western regions are still in the outskirts of the cluster. The ‘nominal’ value of the excess is likely to be $\gtrsim 50$ and thus this cluster can be classified as Abell richness class larger than 0, and probably 1.

We also estimate the cluster richness using the optical CCD data since the K -band area may not be large enough to allow the field galaxy correction to be carried out accurately. The optical CCD data covers a wider area, allowing us to obtain more accurate field counts within the same frame. Here we use another measure of the richness, $N_{0.5}$, a statistic

introduced by Hill & Lilly (1991). This is the count of galaxies within a 0.5 Mpc radius around the cluster and in the magnitude range between m_1 and $m_1 + 3$ (they used an R -band magnitude). They applied the $N_{0.5}$ analysis to the fields around radio galaxies at $z \sim 0.5$. Since the R -band at $z \sim 0.5$ roughly correspond to the I -band at $z \sim 1$, we can make a direct comparison with their measurements. We estimate m_1 for the cluster galaxies to be $I = 21$ mag. As galaxy detection becomes incomplete beyond $I > 23$, we corrected the number counts using the $N(m)$ slope of Tyson (1988). Field galaxy counts are taken from the outer area of our data. The resulting $N_{0.5}$ count is 19–25 for the richest clustering around coordinates (0, –50) in Figure 10. Following the richness calibration by Hill & Lilly (1991), this corresponds to an Abell cluster richness class 1 ($N_{0.5} = 15 \pm 5$ for $R_{\text{Abell}} = 1$), in good agreement with the richness estimated from the K -selected sample.

The estimated richness ($R_{\text{Abell}} \simeq 1$) is consistent with the upper limit of the X-ray Luminosity ($L_x \lesssim 2 \times 10^{44} \text{ erg s}^{-1}$). Only $\approx 10\%$ of the $R_{\text{Abell}} = 1$ and $\approx 20\%$ of the $R_{\text{Abell}} = 2$ clusters have X-ray luminosities above this value (Briel & Henry 1993). Note that the sensitivity of our *ROSAT* observation is such that it would detect the X-ray emission from the Coma cluster ($L_x \approx 5 \times 10^{44} \text{ erg s}^{-1}$, e.g. Briel, Henry, & Böhringer 1992) placed at $z = 1.1$, but it would fail to detect the Virgo cluster at this redshift by a factor of several. An X-ray Multi-Mirror Mission (XMM) observation on this field is planned with an order of magnitude better sensitivity. If the $z = 1.1$ cluster has an X-ray luminosity comparable to the present-day $R_{\text{Abell}} = 1$ –2 clusters, it should be detectable with the XMM observations.

7.2. Blue Galaxy Fraction

Next we examine the blue galaxy fraction of the cluster using both the K -selected and I -selected samples. To study the evolution of the blue-galaxy fraction, Butcher & Oemler (1984) introduced f_b , which is the fraction of bright bluer [$\Delta(B - V) < -0.2$ from the central

color of the C-M relation] galaxies within the R_{30} radius which includes 30% of the total number of cluster members. The f_b values are calculated for absolute-magnitude-limited samples (e.g., $M_V < -20$). This limit is affected by the luminosity evolution of the cluster galaxies, which makes it difficult to compare the f_b values for low- and high-redshift clusters directly. It is also difficult to apply the original criteria directly to our data. Butcher & Oemler (1984) used $B - V$, longwards of the 4000\AA break, while both our R & I bands sample shorter wavelength. Thus, we cannot apply the same criterion of ‘blueness’ as used in Butcher & Oemler (1984). Nevertheless, it is still interesting to quantify the fraction of blue galaxies in an evolutionary sense, i.e., the fraction of galaxies which show signs of star-formation activity when compared with the quiescent members.

First, let us evaluate the blue galaxy fraction using the optical CCD data. We count galaxies within a 0.5 Mpc radius around the center of the clustering and considered the magnitude range of $21 < I < 24$. We set the criterion for *red* galaxies to be $1.3 < R - I < 1.6$ and for *blue* galaxies $0.4 < R - I < 1.3$ on the basis of the model calculation shown in Figure 8. Data for the field correction are taken from the outer area of our optical images. Note that although this criterion does not correspond exactly with that of Butcher & Oemler (1984), it does separate very well quiescent and star-forming galaxies (cf. Figure 8). The resulting blue galaxy fraction of the richest clustering component is $\sim 60\%$, significantly higher than that found in clusters at intermediate redshift. Note, however, that we are selecting galaxies at shorter rest-frame wavelengths than those used by Butcher & Oemler, and therefore our sample is biased towards bluer galaxies when compared with theirs.

In order to estimate f_b using the K -selected ($K < 19$) galaxies, and because of the relatively small area covered by the K -band data, we simply evaluated the fraction of the *blue* galaxies to the total count in the Cluster region relative to the Eastern & Western regions. As before, we call *blue* galaxies those with $R - I < 1.3$. We count 65 galaxies in

the Cluster region, and 15 and 14 galaxies in the Eastern and the Western regions (see Figure 8). On the other hand, there are 54 *blue* galaxies in the Cluster region and 12 and 13 *blue* galaxies in the Eastern and the Western regions. Thus, the nominal blue fraction of the $K < 19$ sample is more than 80%.

Although these estimates are rather crude, they do seem to indicate a very high blue fraction, roughly matching the numbers found for clusters at $z \sim 0.9$ (Postman et al. 1998; Lubin et al. 1998; Rakos & Schombert 1995). If confirmed, they would indicate that the Butcher-Oemler effect continues to increase its strength towards higher redshifts.

7.3. Comparison with Other High-Redshift Clusters

Let us now compare in some detail the photometric properties of our cluster near B2 1335+28 with those of other high-redshift clusters. CIG J0848+4453 at $z = 1.27$ (Stanford et al. 1997) is another good example of $z > 1$ cluster whose photometric properties have been published. It also shows a ‘red finger’ similar to that of our cluster, but the color distribution in $R - K$ of the ‘finger’ galaxies seems to be somewhat tighter. Moreover, their reddest envelope galaxies are ~ 0.5 mag redder in $R - K$ than the predictions of the models discussed in Section 4 when shifted to $z = 1.27$. Considering that the colors of the reddest galaxies in the cluster near B2 1335+28 are marginally bluer than the model predictions, it seems as if the oldest galaxies in CIG J0848+4453 may be older than those in our cluster (taking the redshift difference into account). Note, however, that relatively small uncertainties in the photometric systems and zero-points could accentuate the apparent differences, and it is important to stress that the similarities are probably more significant than the differences between these two clusters.

The optical-NIR colors of the ‘quiescent members’ of our cluster show some scatter,

which we interpreted as possible *age differences* among these passively-evolving galaxies. Another example of a large-scatter C-M relation in a high- z cluster was very recently found by Benítez et al. (1998), who studied the cluster AX J2019+112 at $z = 1.01$ using deep optical-NIR multi-color photometry. There are several galaxies which may define a C-M sequence and they show significant scatter in the VIK two-color diagram, preferentially on the $I - K$ axis. Further examples may be found in da Costa et al. (1999).

Extended X-ray emission has been detected for the clusters CIG J0848+4453 (Stanford et al. 1997) and AX J2019+112 (Benítez et al. 1998; Hattori et al. 1997). If the emission originates from the cluster hot gas, it would suggest that these clusters are dynamically-evolved systems. Strong X-ray emission has not been detected from our cluster, although the sensitivity limit of our data is rather marginal for a cluster with Abell richness class 1, as discussed in §6. The weak concentration and the lumpy and elongated appearance of our cluster may imply that it is dynamically too young to show strong X-ray emission.

The star-formation history of cluster galaxies may well be coupled to the dynamical evolution of the cluster itself. In a morphological study of two $z \sim 0.9$ clusters by Lubin et al. (1998) they found that the fraction of early-type galaxies is higher in the more relaxed and evolved system. In the companion paper, Postman et al. (1998) calculated ‘color ages’ for the galaxies from their $BVRI$ photometric results. The number of galaxies older than 4 Gyr (see Postman et al. for details) is five for CL 1604, the rich and evolved cluster, while none are found for the merging cluster CL 0023. Thus, it is not surprising that in our cluster, which shows many signs of being dynamically young, we also find a large fraction of galaxies with young stellar populations and star-formation activity.

Finally, it is worth mentioning that the our cluster is located in a somewhat unique environment. The quasar B2 1335+28 is one of the members of the quasar concentration

found at $z = 1.1$ by Crampton et al. (1989). Hutchings et al. (1995) found galaxy surface density excess around other quasars in this concentration. If, as it seems likely, the quasars trace an underlying supercluster of galaxies, our cluster would be just a member of this (proto?-)supercluster. It would be extremely interesting to study the overall distribution of the galaxies and their properties over much larger scales, covering the whole quasar concentration.

8. Summary

In this paper we have presented an optical-NIR photometric analysis of the field around the quasar B2 1335+28. Our main findings are:

1. Using some newly-analyzed K -band imaging data, we have examined the galaxy clustering over a larger area than that covered by Yamada et al. (1997). We have confirmed the existence of a fairly rich cluster of galaxies and determined that it extends ~ 90 arcsec in the East-West direction.
2. The cluster contains galaxies with a wide range of colors, but we argue that it is not likely to be heavily contaminated by a foreground cluster. The large scatter of colors is probably intrinsic.
3. Using photometric redshifts, we find a very strong peak at $z \sim 1.1$. No spectroscopic redshifts are yet available. From the spatial coincidence of the narrow-band-selected ([OII]-emitting) galaxies and the K -selected candidate cluster galaxies, we conclude that the redshift of the cluster is probably $z = 1.1$, similar to that of the quasar.
4. There is only a small fraction of galaxies which have colors consistent with passive-evolution models. Substantial numbers of red galaxies with some UV excess (bluer

$R - I$ color) as well as bluer galaxies with colors similar to those of mildly-evolving disk galaxy models have been found. These bluer galaxies may be the precursors of the galaxies with post-starburst features frequently seen in clusters at intermediate redshifts.

5. The Abell richness of the cluster is $R_{\text{Abell}} \sim 1$. Although our *ROSAT* HRI data set an upper limit ($2 \times 10^{44} \text{ erg s}^{-1}$) to any possible extended X-ray emission from the cluster, this is still consistent with the estimated richness.
6. The blue galaxy fraction is 60–80%, substantially larger than that of $z \lesssim 0.5$ clusters, but comparable to other $z \sim 1$ clusters. This suggests that the strength of the Butcher-Oemler effect continues to grow with redshift.
7. By selecting passively-evolving galaxies using a rest-frame UV color criterion, we recover a clear optical-NIR color-magnitude sequence which may be the precursor of the tight C-M relations seen in lower-redshift clusters. The C-M slope is consistent with passive-evolution models, while its scatter is fairly large (~ 0.2 mag in $R - K$). The mean age of these galaxies is estimated to be ~ 2 Gyr at the epoch of observation, although the absolute value is somewhat uncertain due to the size of the photometric zero-point errors.
8. Using R and I -band images covering a wider field, we examine the large-scale distribution of the galaxies with similarly red $R - I$ colors to those of the cluster galaxies in the K -selected sample. Some ‘lumpy’ and elongated structures are revealed, including an extension of the cluster in the South-West direction. This result suggests that the cluster is still dynamically young and may evolve into a larger cluster in the future.

This research was partially supported by grants-in-aid for scientific research of the Japanese Ministry of Education, Science, Sports and Culture (08740181, 09740168). Part of this work was also supported by the Foundation for the Promotion of Astronomy of Japan. We thank E.F. Bell and R.G. Bower for allowing us to use the Kodama et al's (1999) photometric redshift code in this paper. A.A.S. acknowledges generous financial support from the Royal Society. T.K. thanks the JSPS postdoctoral fellowship for research abroad for financial support. T.M. thanks the JSPS Japan-Germany Collaboration for High-Energy Astrophysics Program for travel support to Tohoku University, where most of the X-ray analysis was carried out. T.M. also thanks Tohoku University for their hospitality during his visit. K.O. thanks the Institute of Astronomy, University of Hawaii, where part of this work was done, for their hospitality during his stay. T.Y., A.A.S., and T.K. would like to thank the International Program for Advanced Studies in Astrophysics “Guillermo Haro”, hosted by the Instituto Nacional de Astrofísica, Óptica y Electrónica (INAOE, Mexico) for their hospitality during the summer of 1998, when many of the results presented here were discussed.

REFERENCES

- Abell, G. O. 1958, *ApJS*, 3, 211
- Abraham, R. G., Smecker-Hane, T. A., Hutchings, J. B., Carlberg, R. G., Yee, H. K. C., Ellingson, E., Morris, S., Oke, J. B., & Rigler, M. 1996, *ApJ*, 471, 694
- Aragón-Salamanca, A., Ellis, R. S., Couch, W. J., & Carter, D. 1993, *MNRAS*, 262, 764
- Arnaud, K. A. 1996, in *ASP Conf. Ser. 101, Astronomical Data Analysis Software and Systems V*, eds. Jacoby, G. H., & Barne, J., 17
- Barger, A. J., Aragón-Salamanca, A., Ellis, R. S., Couch, W. J., Smail, I., & Sharples, R. M. 1996, *MNRAS*, 279, 1
- Beers, T.C., Flynn, K., & Gebhard, K. 1990, *AJ*, 100, 32
- Benítez, N., Broadhurst, T., Rosati, P., Courbin, F., Squires, G., Lidman, C., & Magain, P. 1998, *ApJ*, submitted (astro-ph/9812218)
- Bertin, E., & Arnouts, S. 1996, *A&AS*, 117, 393
- Bessel, M. S. 1990, *A&AS*, 83, 357
- Bower, R. G., Lucey, J. R., & Ellis, R. S. 1992, *MNRAS*, 254, 601
- Bower, R. G., Kodama, T., & Terlevich, A. 1998, *MNRAS*, 299, 1193
- Briel, U. G., Henry, J. P., & Böhringer, H. 1992, *A&A*, 259, L31
- Briel, U. G., & Henry, J. P. 1993, *A&A*, 278, 379
- Burstein, D., & Heiles, C. 1982, *AJ*, 87, 1165
- Butcher, H., & Oemler, A. Jr. 1978, *ApJ*, 226, 559
- Butcher, H., & Oemler, A. Jr. 1984, *ApJ*, 285, 426
- Colla, G., Fanti, C., Fanti, R., Ficarra, A., Formiggini, L., Gandolfi, E., Lari, C., Marano, B., Padrielli, L., & Tomasi, P. 1972, *A&AS*, 7, 1

- Couch, W. J., & Sharples, R. M. 1987, MNRAS, 229, 423
- Couch, W. J., Ellis, R. S., Sharples, R. M., & Smail, I. 1994, ApJ, 430, 121
- Couch, W. J., Barger, A. J., Smail, I., Ellis, R. S., & Sharples, R. M. 1998, ApJ, 497, 188
- Cowie, L., Songaila, A., Hu, E., & Cohen, J. G. 1996, AJ, 112, 839
- Crampton, D., Cowley, A. P., & Hartwick, F. D. A. 1989, ApJ, 345, 59
- da Costa, L., Scodreggio, M., Olsen, L.F., Nonino, M., Rengelink, R., Bender, R., Franx, M.,
Jørgensen, H.E., Renzini, A., & Rosati, P. 1999, A&A, 343, L29
- David, L. P., Jones, C., & Forman, W. 1996, ApJ, 473, 692
- Davis, L. 1987, Specifications for the Aperture Photometry Package, NOAO
- Dickey, J. M., & Lockman, F. J. 1990, ARA&A, 280, 215
- Dickson, M. 1995, in ASP Conf. Proc. 86, Fresh Views of Elliptical Galaxies, eds. A.
Buzzini, A. Renzini, & A. serrano (San Francisco: ASP), 283
- Dressler, A., Thompson, I. B., & Sackett P. A. 1985, ApJ, 288, 481
- Dressler, A., & Gunn, J. E. 1992, ApJS, 78, 1
- Dressler, A., Oemler, A. Jr., Couch, W., Smail, I., Ellis, R. S., Barger, A., Butcher, H.,
Poggianti, B. M., & Sharples, R. M. 1997, ApJ, 490, 577
- Ellis, R. S., Smail, I., Dressler, A., Couch, W. J., Oemler, A. Jr., Butcher, H. R., &
Sharples, R. M. 1997, ApJ, 483, 582
- Gardner, J. P. 1995, ApJS, 98, 441
- Gladders, M. D., López-Cruz, O., Yee, H. K. C., & Kodama, T. 1998, ApJ, 501, 571
- Glazebrook, K., Blake, C., Economou, F., Lilly, S., & Colless M. 1998, MNRAS, submitted
(astro-ph/9808276)
- Hall, P. B., & Green, R. F. 1998, ApJ, 507, 558

- Hattori, M., Ikebe, Y., Asaoka, I., Takeshima, T., Boeringer, H., Mihara, T., Neumann, D. M., Schindler, S., Tsuru, T., & Tamura, T. 1997, *Nature*, 388, 146
- Hill, G. J., & Lilly, S. J. 1991, *ApJ*, 367, 1
- Hutchings, J. B., Crampton, D., & Persram, D. 1993, *AJ*, 106, 1324 (H93)
- Hutchings, J. B., Crampton, D., & Johnson, A. 1995, *AJ*, 109, 73
- Johnson, H. L. 1966, *ARA&A*, 4, 193
- Kennicutt R. C. 1992, *ApJS*, 79, 255
- Kodama, T., & Arimoto, N. 1997, *A&A*, 320, 41 (KA97)
- Kodama, T., Bell E. F., & Bower R. G. 1999, *MNRAS*, 302, 152
- Kodama, T., Arimoto, N., Barger, A. J., & Aragón-Salamanca, A. 1998, *A&A*, 334, 99
- Kuntschner, H., & Davis, R. L. 1998, *MNRAS*, 295, L29
- Landolt, A. U. 1992, *AJ*, 104, 340
- Lilly S. J. et al. 1998, *ApJ*, 500, 75
- Lubin, L. M., Postman, M., Oke, J. B., Ratnatunga, K. U., Gunn, J. E., Hoessel, J. G., & Schneider, D. P. 1998, *AJ*, 116, 584
- Minezaki, T., Kobayashi, Y., Yoshii, Y., & Peterson, B. A. 1998, *ApJ*, 494, 111
- Morris, S., Hutchings, J. B., Carlberg, R. G., Yee, H. K. C., Ellingson, E., Balogh, M. L. Abraham, R. G., & Smecker-Hane, T. A. 1998, *ApJ*, 507, 84
- O’Connell, R. 1988, in *Towards Understanding Galaxies at Large Redshift*, eds. Renzini, A., & Kron, R. G. (Kluwer Academic Publishers), p. 177
- Oemler, A. Jr., Dressler, A., & Butcher, H. 1997, *ApJ*, 474, 561
- Olsen, L. F. et al. 1999, *A&A*, 345, 363
- Ostrander, E. J., Nichol R. C., Ratnatunga K. U., & Griffiths R. E. 1998, *AJ*, 116, 2644

- Poggianti, B. M., Smail, I., Dressler, A., Couch, W. J., Barger, A. J., Butcher, H., Ellis, R. S., & Oemler, A. Jr. 1999, ApJ, in press (astro-ph/9901264)
- Postman, M., Lubin, L. M., Gunn, J. E., Oke, J. B., Hoessel, J. G., Schneider, D. P., & Christensen, J. A. 1996, AJ, 111, 615
- Postman, M., Lubin, L. M., & Oke, J. B. 1998, AJ, 116, 560
- Racos, K. D., & Schombert J. M. 1995, ApJ, 439, 47
- Savage, B. D., & Mathis, J. S. 1979, ARA&A, 17, 73
- Sawicki, M., & Yee, H. K. C. 1998, AJ, 115, 1329
- Smail, I., Edge, A. C., Ellis, R. S., & Blandford, R. D. 1998, MNRAS, 293, 124
- Stanford, S. A., Elston, R., Eisenhardt, P. R., Spinrad, H., Stern, D., & Dey, A. 1997, AJ, 114, 2232
- Stanford, S. A., Eisenhardt, P. R., & Dickinson, M. 1998, ApJ, 492, 461
- Tyson, J. A. 1988, AJ, 96, 1
- van Dokkum, P. G., Franx, M., Kelson, D. D., Illingworth, G. D., Fisher, D., & Fabricant, D. 1998, ApJ, 500, 714
- Véron-Cetty M. -P., & Véron P. 1996 A&AS, 115, 97
- Yamada, T., Tanaka, I., Aragón-Salamanca, A., Kodama, T., Ohta, K., & Arimoto, N. 1997, ApJ, 487, L125 (*Paper I*)

Fig. 1.— A schematic illustration of the imaged fields.

Fig. 2.— Three-color representation of the field around the quasar B2 1335+28. The Blue, Green and Red images correspond to the R -, I - and K -band frames, respectively. North is up, and East is left. The absolute magnitude of the quasar is $M_V \sim -24$. The galaxy G1 is the reddest and brightest galaxy in the cluster, and G2 is the reddest [OII] emitter detected by Hutchings et al. (1993). A red patch in lower-left corner is a ghost.

Fig. 3.— The number counts of the objects in each frame. Panel (a): The R -band number counts. Panel (b): the I -band counts. Filled and open circles represent the counts in the Cluster region and the Western region defined in the K -band frame (see Figure 1). Dashed lines in panel (a) & (b) represent the counts in the complete optical images excluding the area of the K -band *Paper I* frames and around two bright stars. The ratios of these three areas are 1:1:13. Stars are not rejected from these counts. Panel (c): K -band number counts for the *Paper I* frame. Panel (d): K -band counts for the EAST frame. Filled circles show the counts in the Cluster region and open ones in the Western (c) and the Eastern (d) region. The dashed line shows the K -band galaxy counts for the South Galactic Pole by Minezaki et al. (1998). Stars are rejected from the counts in (c) and (d). Comparing panels (c) and (d), we see that they are well matched to $K = 19$.

Fig. 4.— The distribution of $K < 19$ objects in the field. Coordinates are offsets from the quasar in arcsecs. North is up and East is left. Large filled circles, small filled circles and small open circles represent the objects with $R - K > 5$, $4 < R - K < 5$, and $R - K < 4$, respectively. Asterisks are objects that are consistent with stars in both FWHM and colors.

Fig. 5.— Photometric redshift distribution using Kodama, Bell & Bower (1998) method. We show all the objects in the Cluster region ($3' \times 1.5'$ area) with $K < 19$ mag (solid line).

As a reference, the observed redshift distribution of $K < 19$ field galaxies from Cowie et al. (1996) is shown after scaling by area (dashed line).

Fig. 6.— $R-K$ versus K color-magnitude diagram for the K -selected galaxies. Filled circles, open circles, and open boxes represent the objects in the Cluster region, the Western region, and the Eastern region, respectively (see Figure 1). The model tracks shown as a thick solid line, thin solid line, and dashed line are the “Coma C-M model” with formation epochs (z_f) of 4.4, 2.4 and 1.6 respectively (see text, KA97). Evolutionary models with different masses ($M_V = -22$ and -18.5 mag at $z = 0$) are shown.

Fig. 7.— $I-K$ versus $R-I$ two-color diagram for all objects brighter than $K = 19$. The symbols are the same as in Figure 6. The symbols with large diamonds correspond to the emission-line galaxies found by H93. The model tracks shown as “Coma C-M model” are the same ones used in Figure 6. The exponentially-decaying SFR models with time scales $\tau = 1$ and 4 Gyr are also plotted. The asterisk shows the color of a 0.5 Gyr constant star formation model observed at $z = 1.1$. The effect of internal extinction and that of an $EW = 100\text{\AA}$ emission line in the I -band are shown as arrows in the bottom-right corner. See text for details.

Fig. 8.— The same as Figure 7, but with models in which various amounts of a star-forming component are added to the passively-evolving old component (see text). The passive models are shown again as thick lines. The old+star-forming tracks (thin lines) are for galaxies of different metallicity/luminosity: the upper line is for a bright metal-rich model and the lower for a faint metal-poor one following the “Coma C-M model” of KA97. The f_{burst} values indicate the mass fraction in the star-forming component (equation 1).

Fig. 9.— The “recovered” C-M sequence for the cluster galaxies (see text; 9a for K vs $R-K$ and 9b for K vs $I-K$). Circles, squares, and triangles represent galaxies in the Cluster

region, the Western region, and the Eastern region, respectively. The symbols with small filled circles show the galaxies having colors consistent with the passive evolution model and without UV excess. The dashed line shows the predicted C-M relation at $z = 1.1$ ($z_f = 4.4$). The solid lines are the $z = 1.1$ colors of the “Coma C-M model” for ages between 0.5 Gyr and 7 Gyr (Note that the age of the universe at $z = 1.1$ is 4.3 Gyr in our cosmology). The results for two different mass/metallicity models ($M_V = -22$ and -18.5) are shown.

Fig. 10.— The distribution of the $I < 23.5$ galaxies on the CCD frame. A linear scale of 100 arcsec corresponds to about 0.85 Mpc at the quasar redshift in our adopted cosmology. Filled circles are objects with $21 < I < 23.5$ and $0.8 < R - I < 1.3$ (small filled circles) and $R - I > 1.3$ (large filled circles). Faint bluer objects ($21 < I < 23.5$ and $R - I < 0.8$) are shown as small open circles. The large open circles are bright ($I < 21$) galaxies. The object coordinates are relative offsets from the quasar in arcsec. The dashed rectangle shows the area of K -band frames. Two large gray patches are the regions affected by bright stars and thus excluded. Stars brighter than $I = 21$ are removed, but fainter ones are not removed because the star-galaxy separation is not robust for fainter objects.

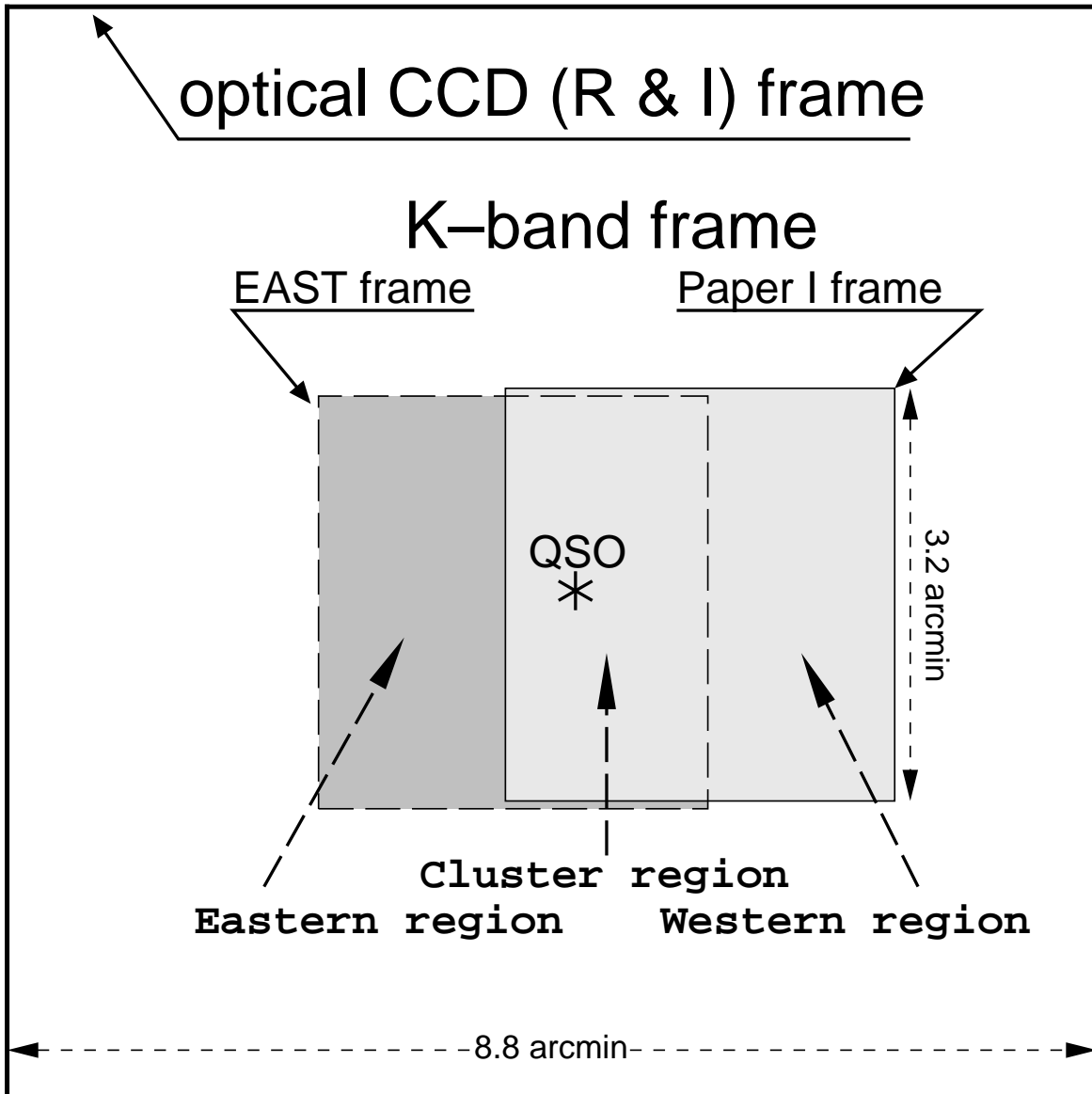


Figure 1.

Figure 2: COLOR IMAGE AVAILABLE AT <http://xxx.lanl.gov/archive/astro-ph>

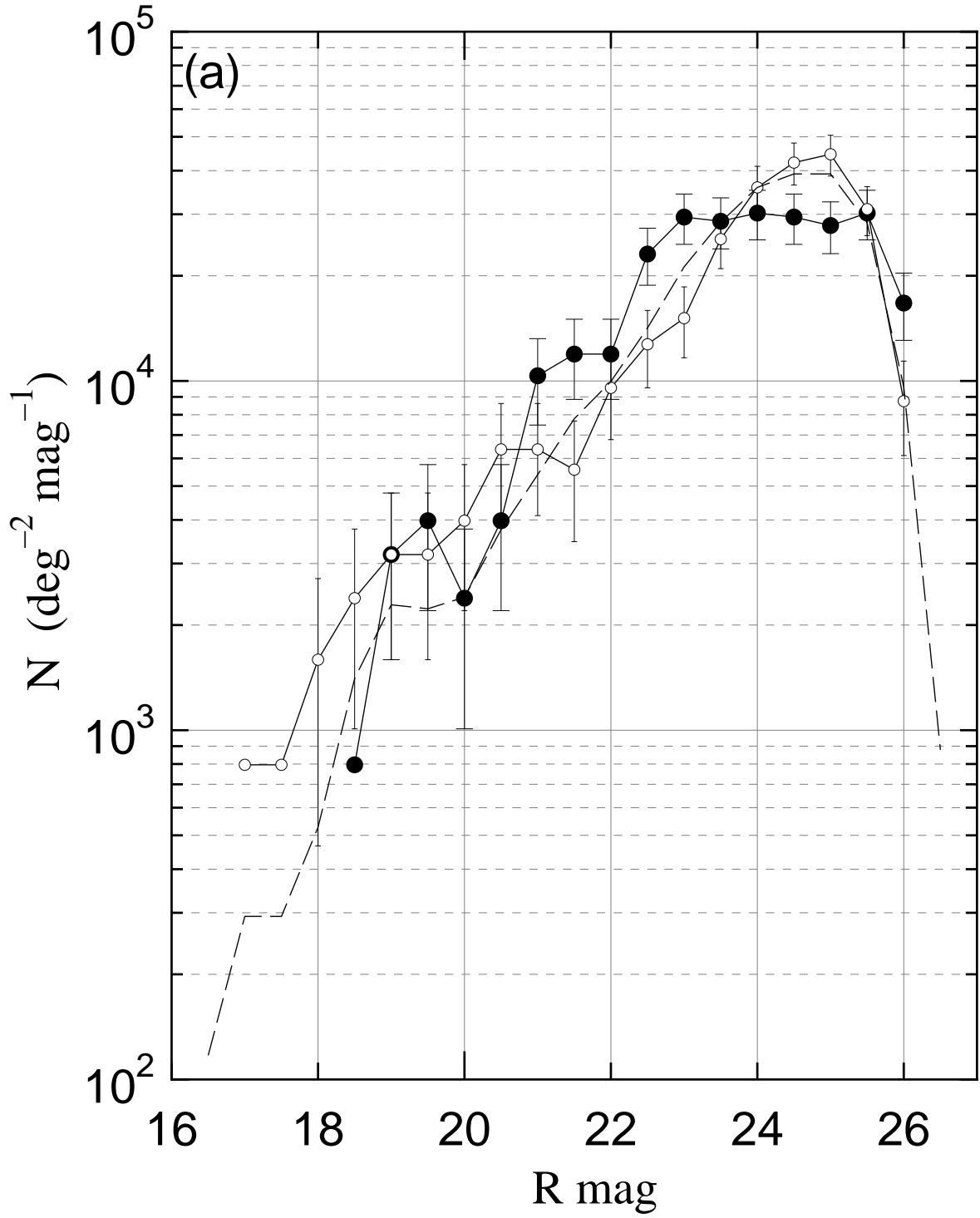


Figure 3a.

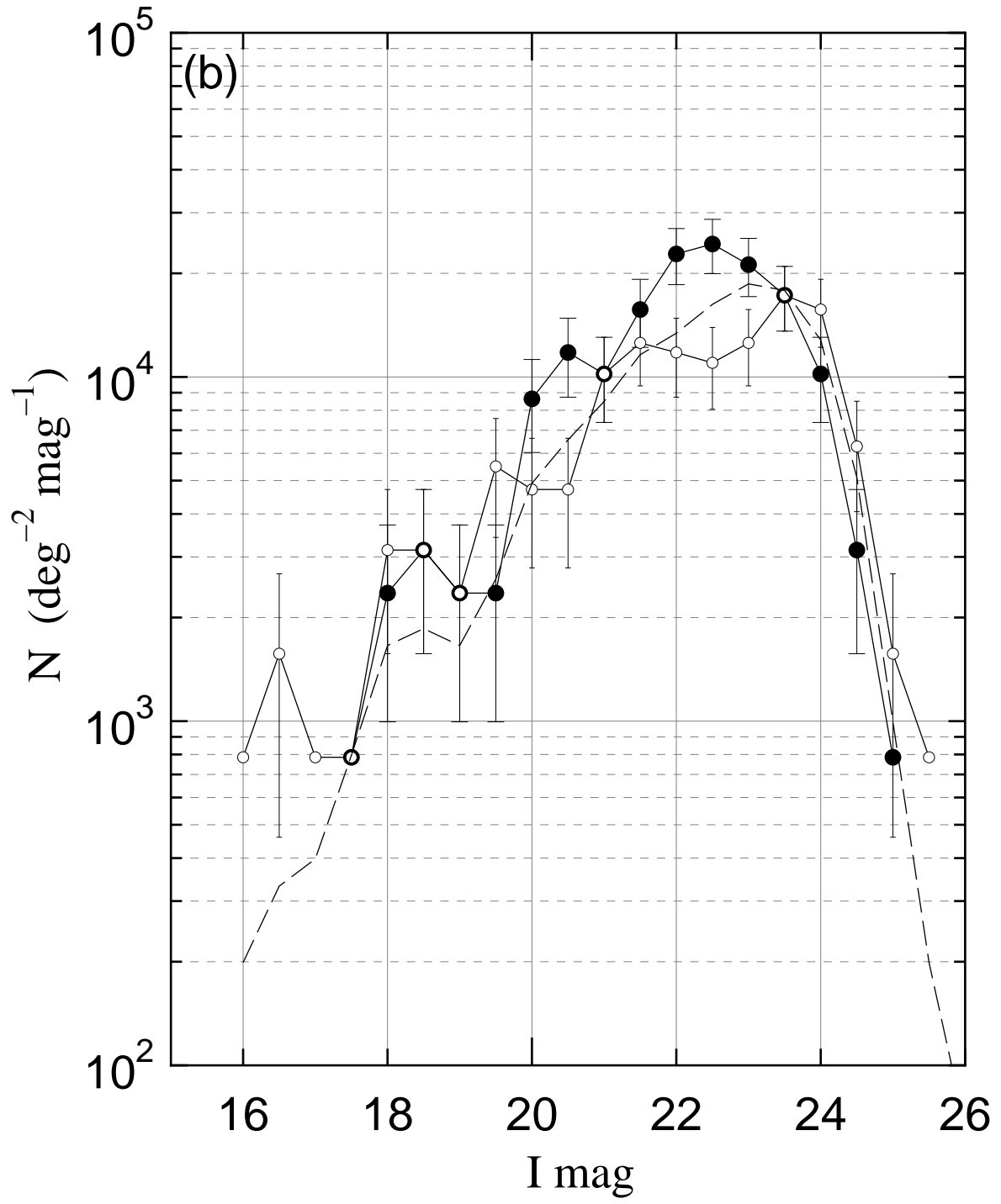


Figure 3b.

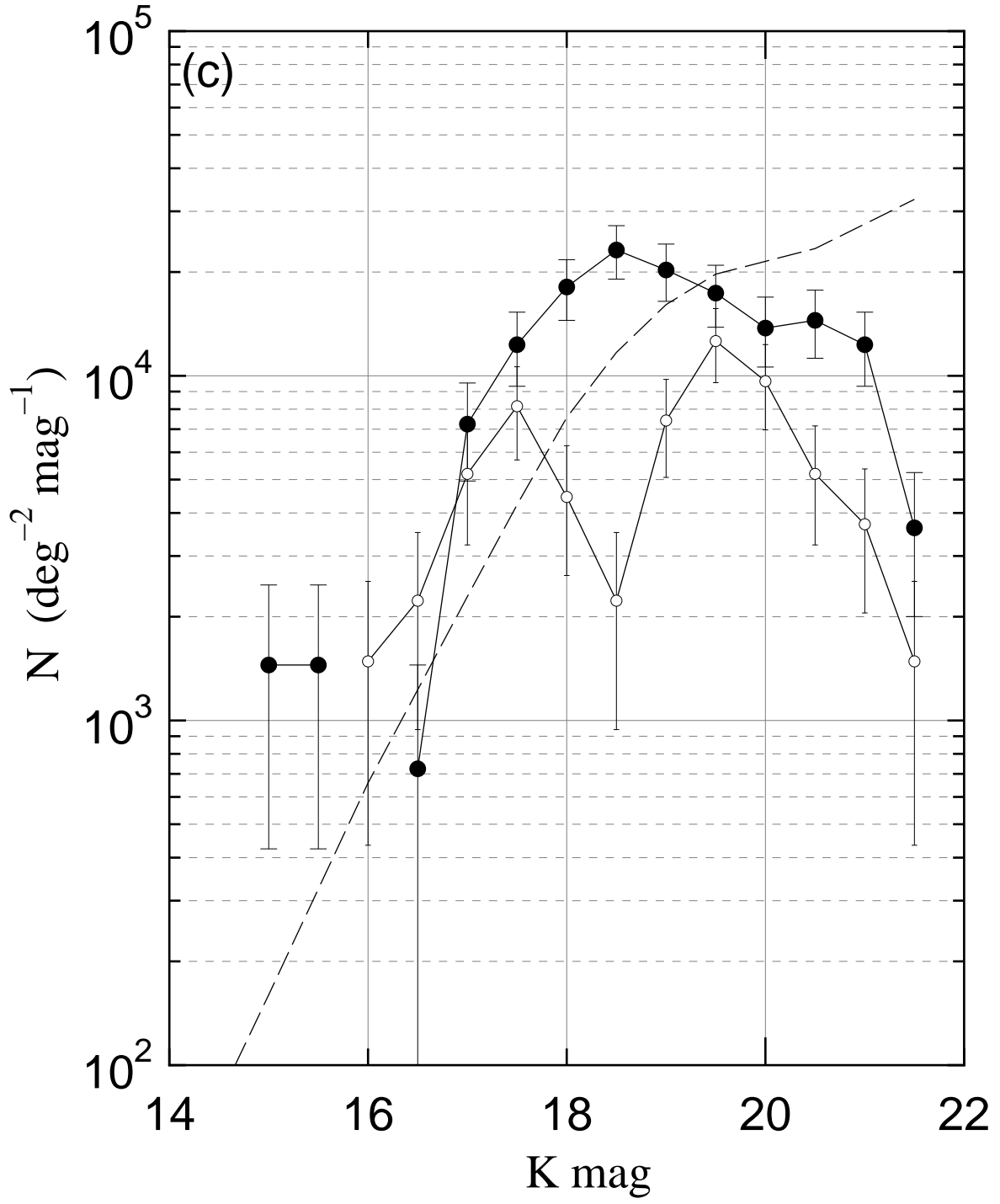


Figure 3c.

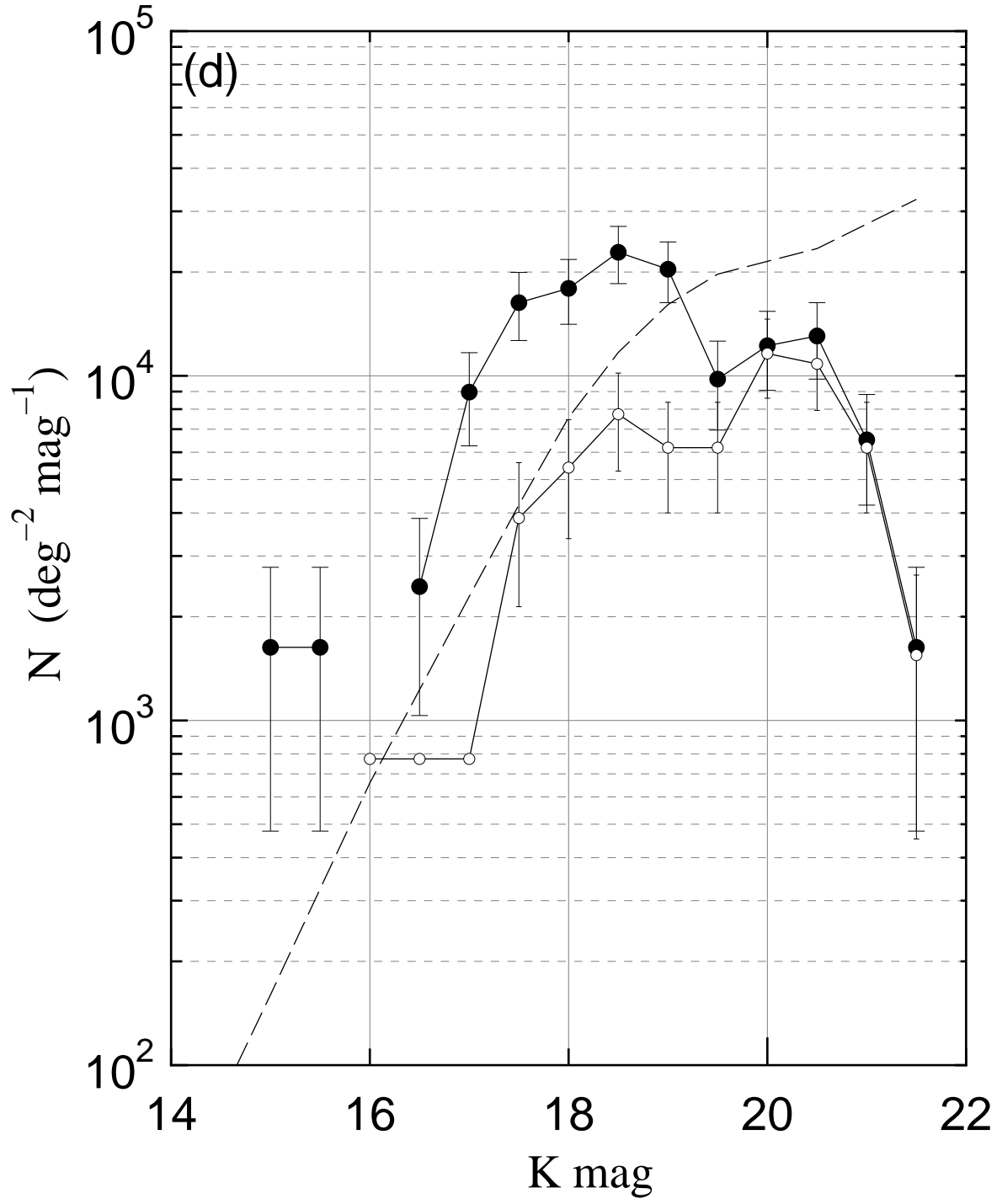


Figure 3d.

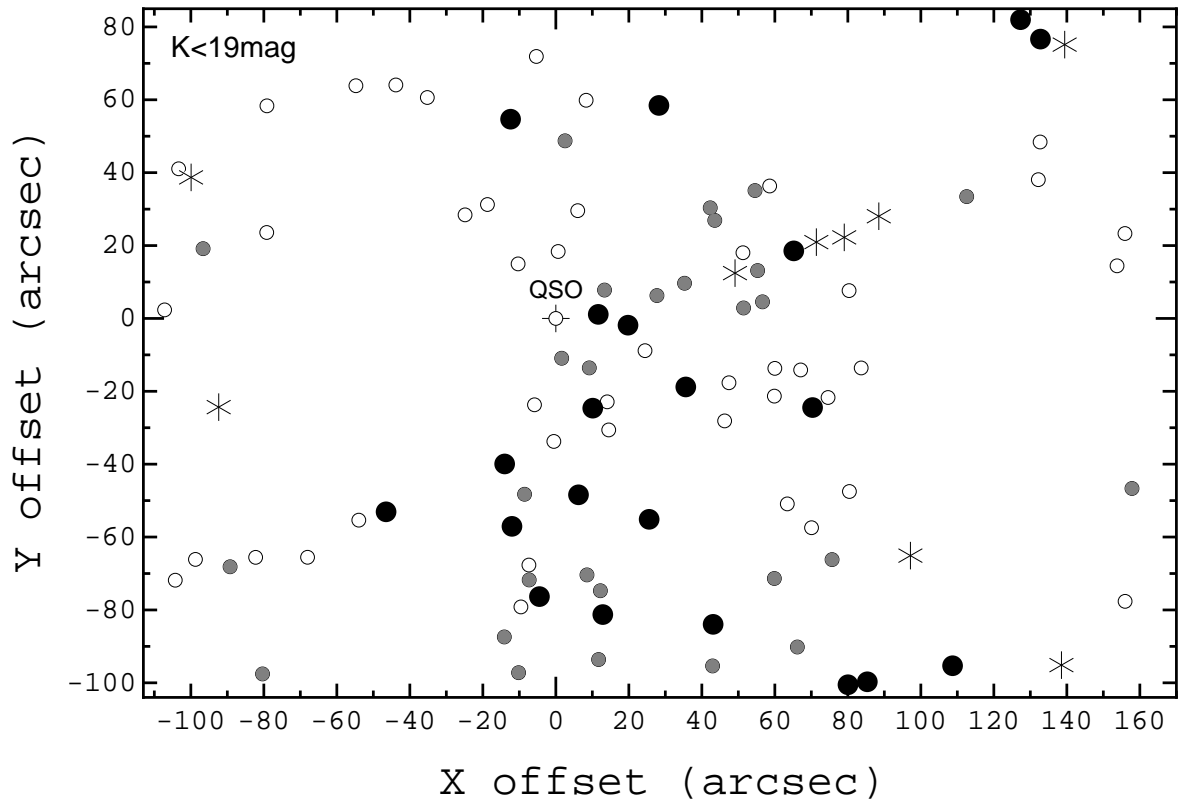


Figure 4.

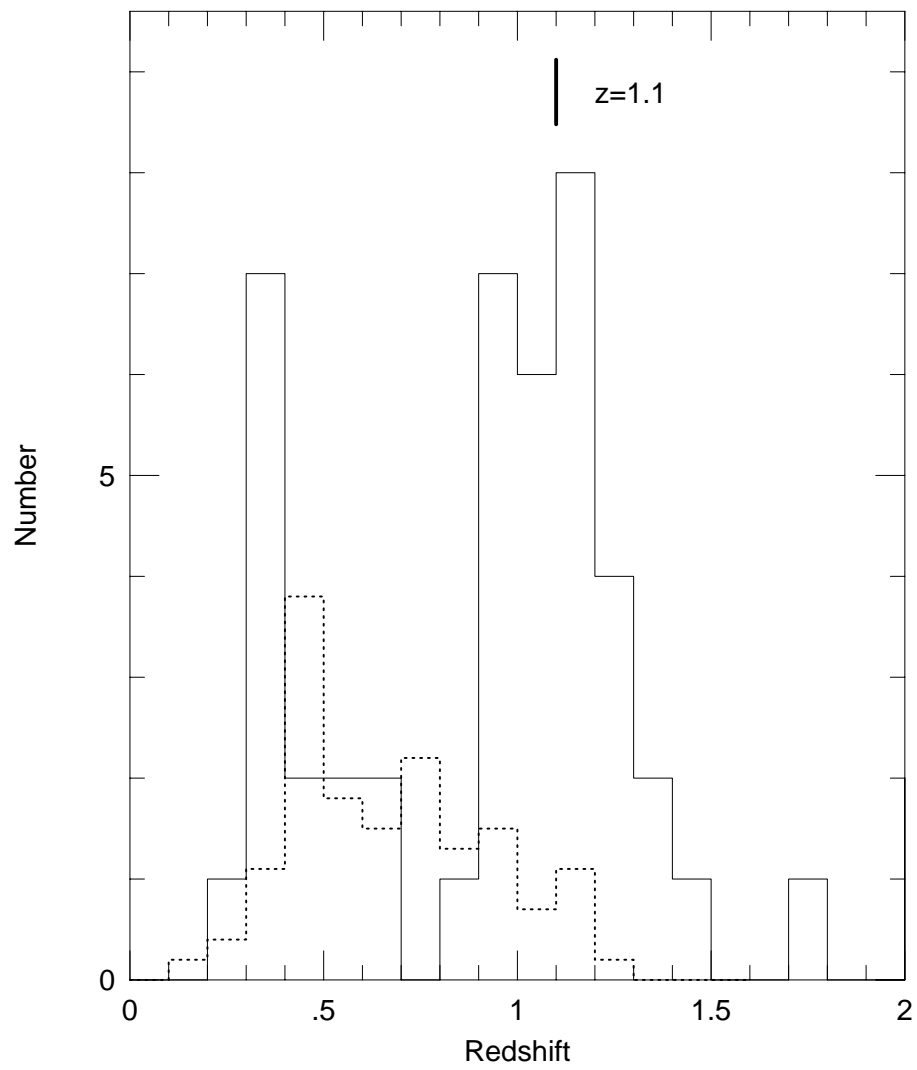


Figure 5.

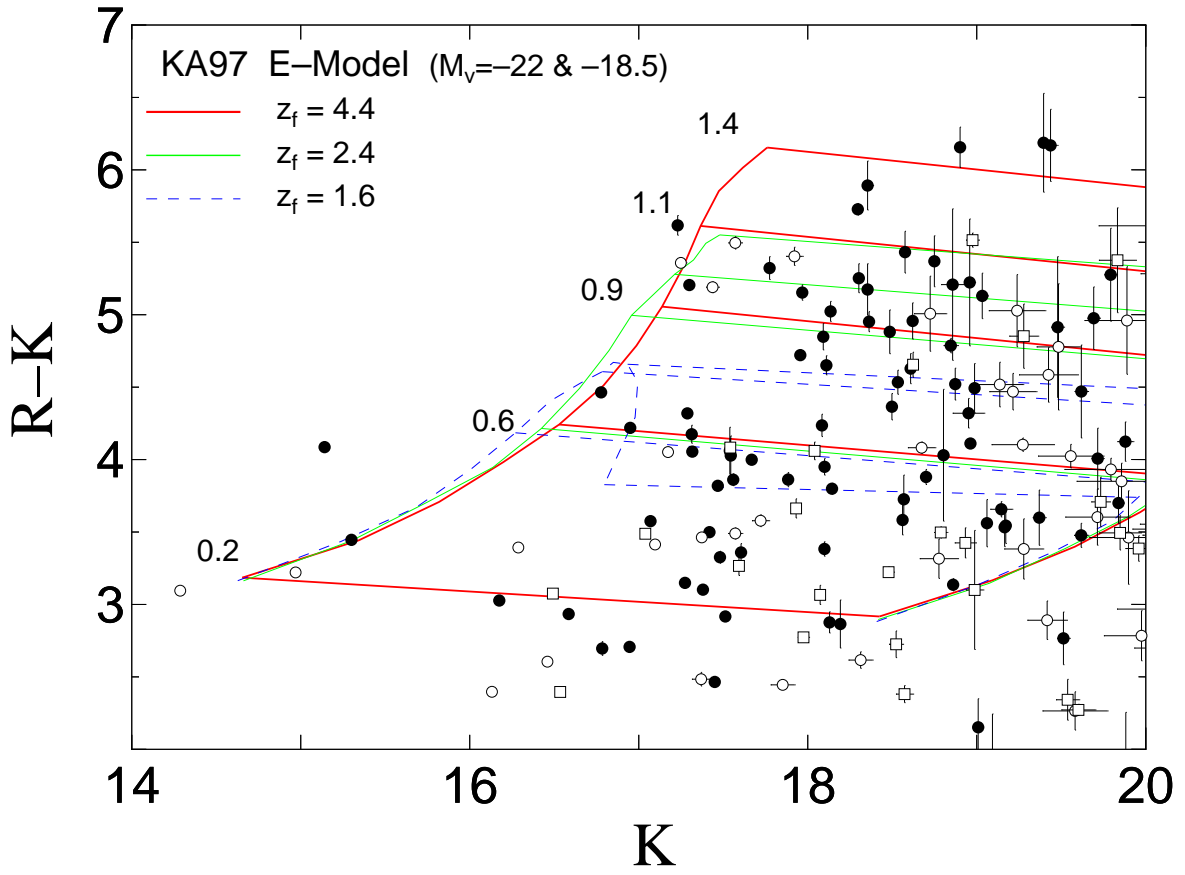


Figure 6.

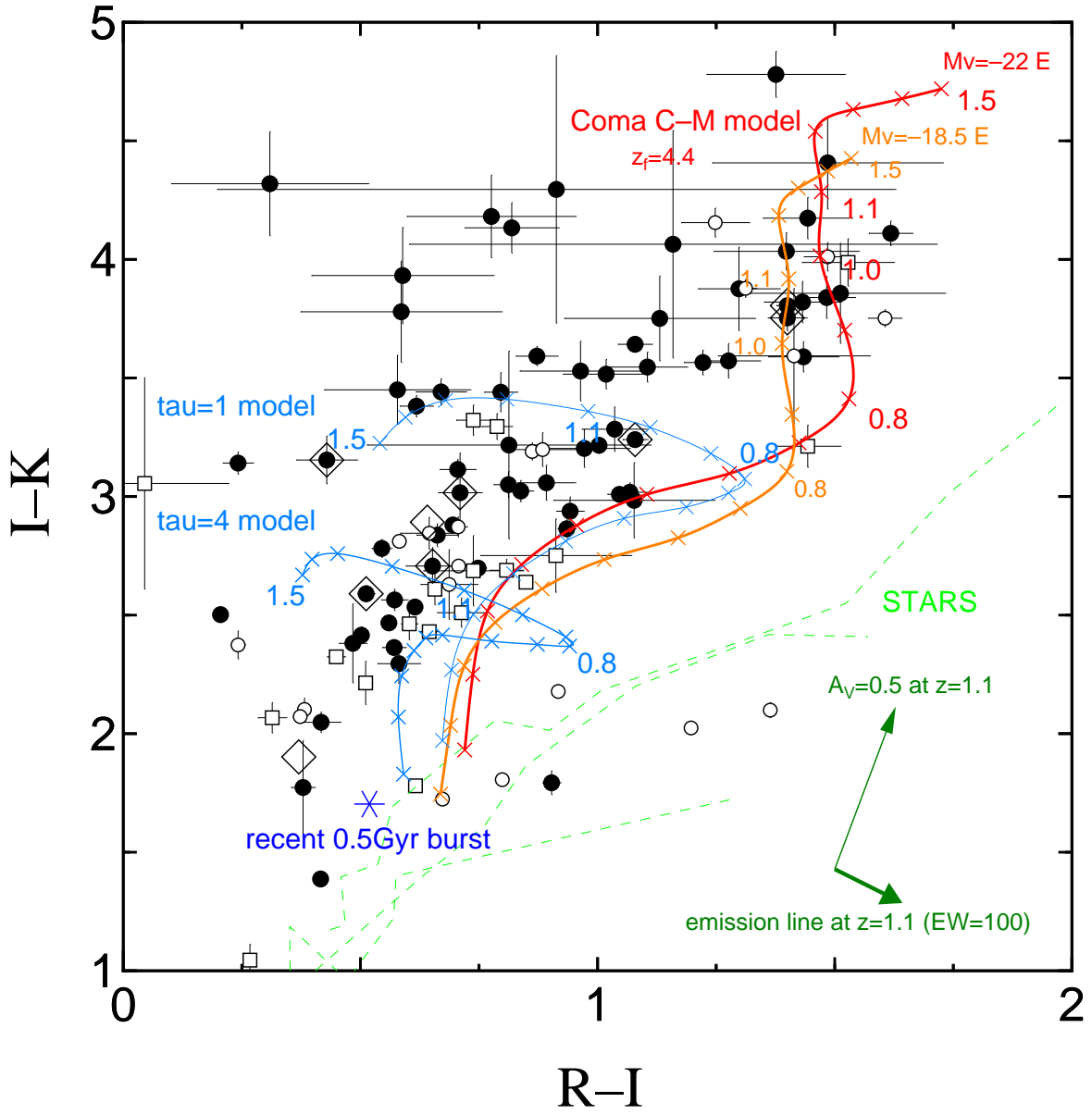


Figure 7.

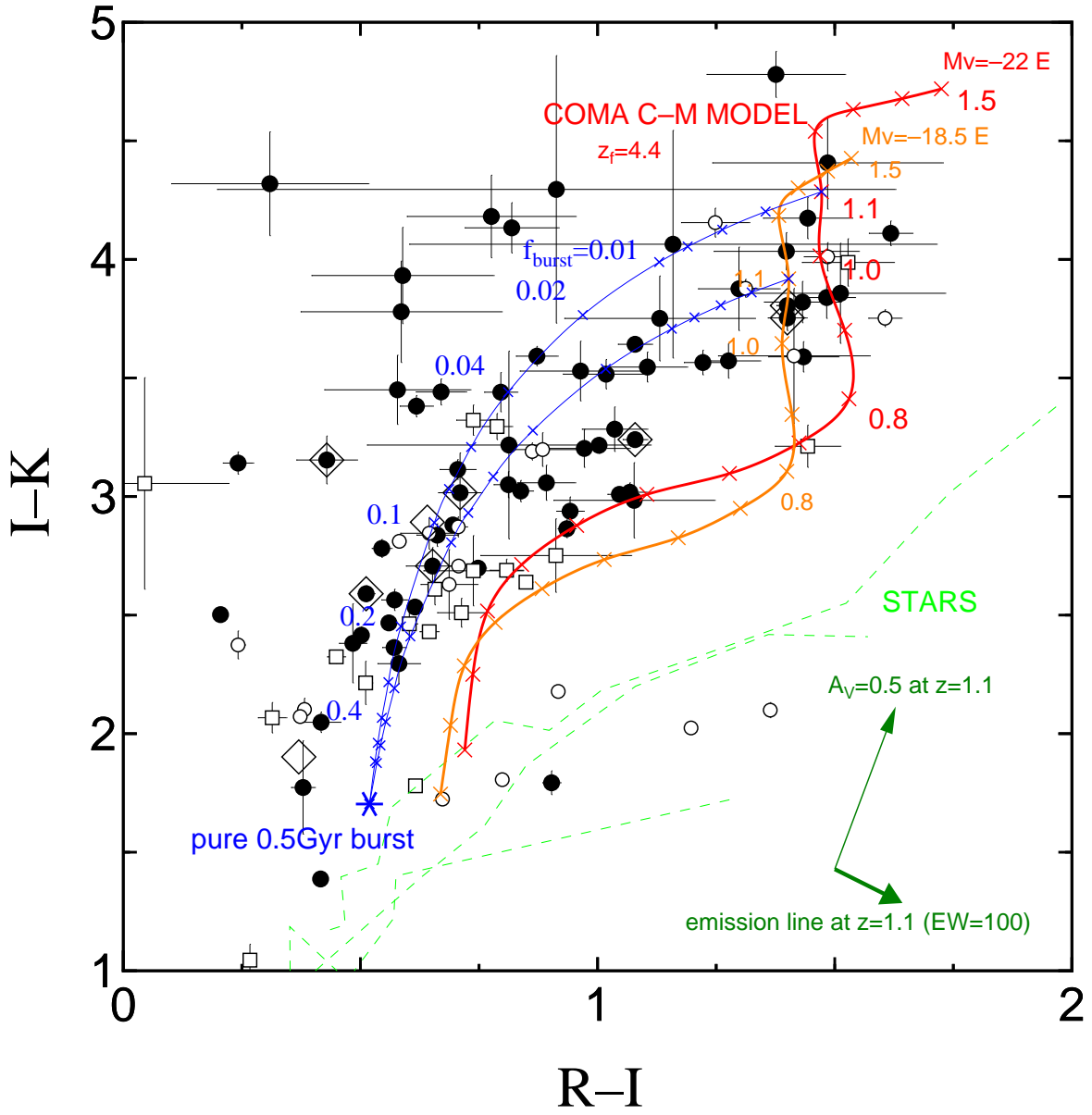


Figure 8.

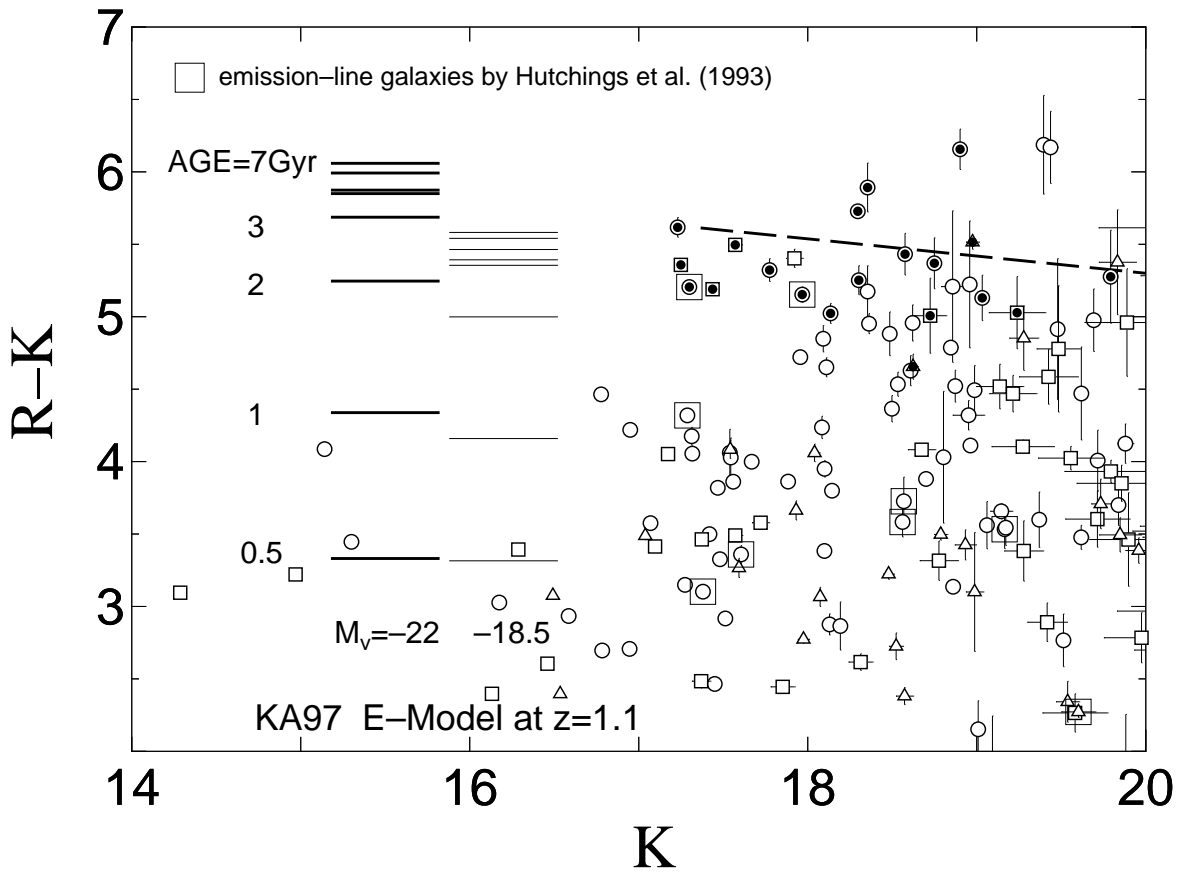


Figure 9a.

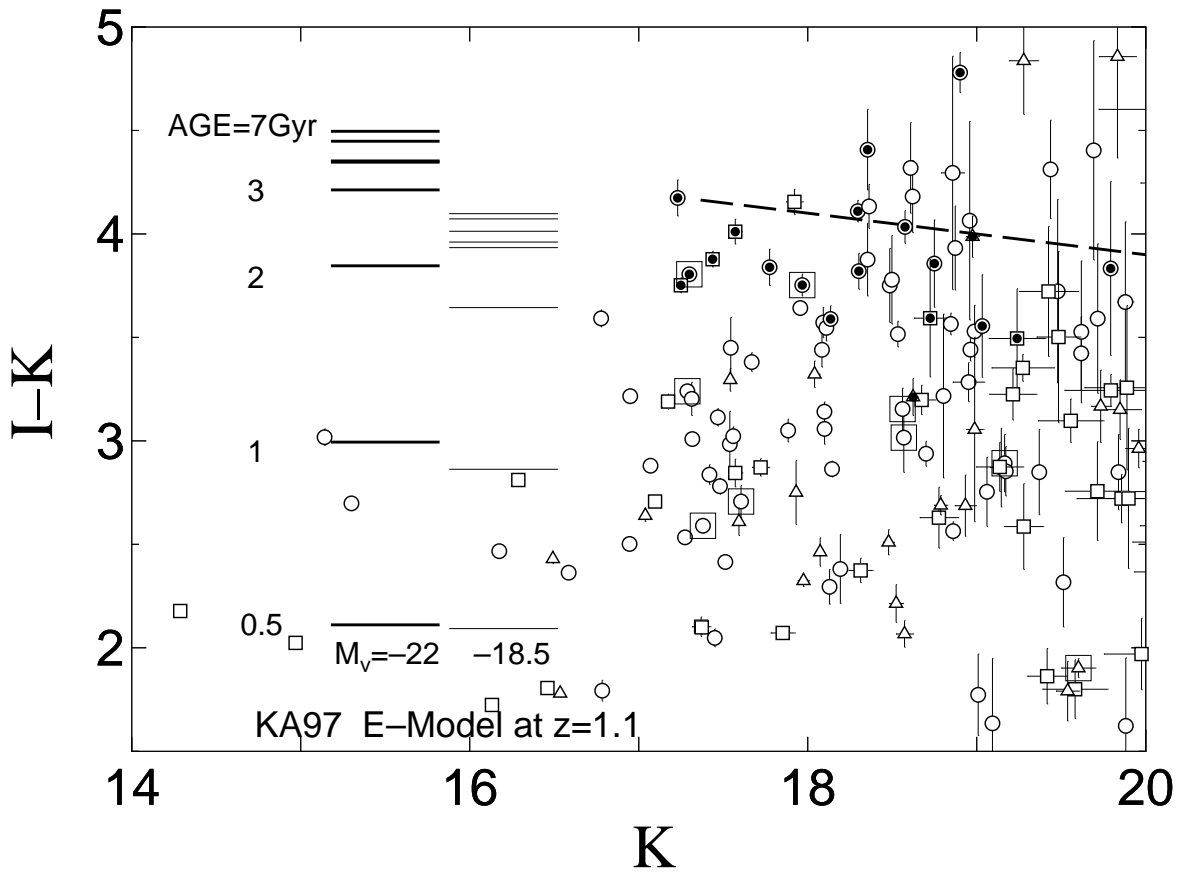


Figure 9b.

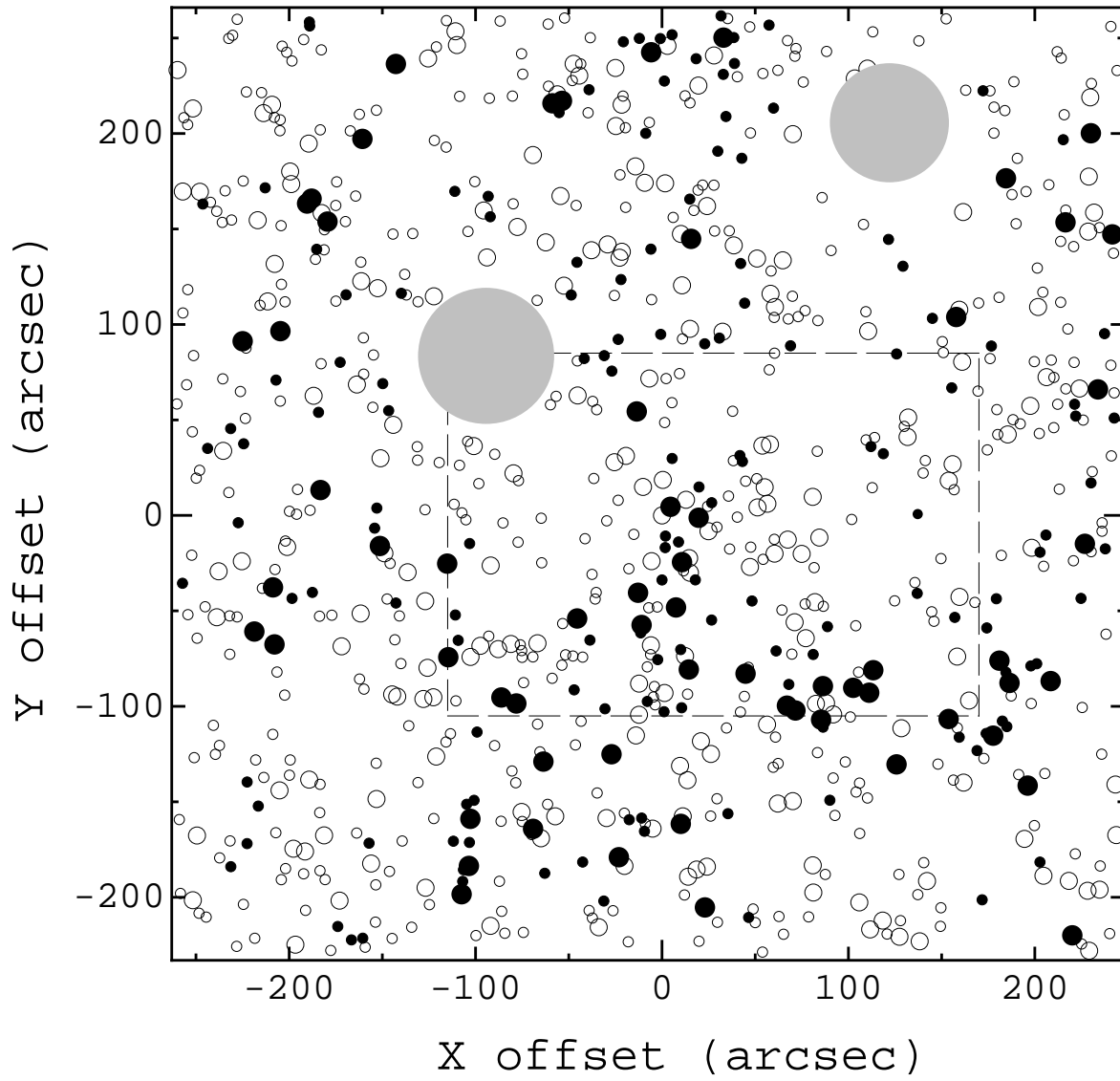


Figure 10.

Table 1. K -selected object catalog.

ID ^a	X''_{QSO} ^b	Y''_{QSO} ^b	K_{MB} ^c	$R - I$ ^d	error	$R - K$ ^d	error	$I - K$ ^d	error
1001	300.2	24.2	15.14	1.07	0.04	4.09	0.04	3.02	0.04
1002	317.4	-113.1	15.30	0.75	0.02	3.45	0.02	2.70	0.02
1003	355.6	-74.9	16.17	0.56	0.01	3.03	0.02	2.47	0.02
1004	-131.9	150.7	16.59	0.57	0.03	2.93	0.02	2.36	0.03
1005	401.2	-350.9	16.78	0.87	0.04	4.46	0.03	3.59	0.04
1006	260.3	66.0	16.78	0.90	0.02	2.70	0.05	1.79	0.05
1007	0.0	0.0	16.95	0.21	0.01	2.71	0.03	2.50	0.03
1008	70.7	41.3	16.95	1.00	0.01	4.22	0.03	3.22	0.03
1009	245.2	-149.1	17.07	0.70	0.01	3.58	0.02	2.88	0.02
1010	378.4	111.1	17.20	0.42	0.01	1.80	0.02	1.39	0.02
1011	104.8	-9.8	17.23	1.44	0.09	5.62	0.07	4.17	0.09
1012	395.4	-115.0	17.27	0.62	0.02	3.15	0.02	2.53	0.02
1013	-74.9	-463.4	17.29	1.08	0.03	4.32	0.03	3.24	0.03
1014	-74.4	-211.7	17.30	1.40	0.02	5.21	0.02	3.81	0.02
1015	272.7	15.2	17.31	0.97	0.10	4.18	0.06	3.20	0.08
1016	289.3	186.2	17.32	1.05	0.03	4.06	0.03	3.01	0.02
1017	-28.3	381.3	17.38	0.51	0.02	3.10	0.03	2.59	0.03
1018	-54.8	79.4	17.42	0.66	0.04	3.50	0.02	2.84	0.05
1019	3.4	97.5	17.45	0.42	0.04	2.47	0.04	2.05	0.04
1020	-99.4	165.8	17.47	0.71	0.04	3.82	0.02	3.11	0.04
1021	-39.2	-358.8	17.48	0.55	0.02	3.33	0.04	2.78	0.04
1022	-31.0	-125.6	17.51	0.50	0.01	2.92	0.04	2.42	0.04
1023	293.0	69.7	17.54	1.08	0.17	4.06	0.16	2.98	0.16
1024	64.7	-396.2	17.54	0.58	0.15	4.03	0.14	3.45	0.15
1025	310.6	192.7	17.56	0.84	0.03	3.86	0.04	3.02	0.05
1026	76.8	-162.2	17.61	0.65	0.06	3.36	0.06	2.71	0.08
1027	-50.8	-419.7	17.67	0.62	0.04	4.00	0.03	3.38	0.05
1028	32.9	-256.6	17.77	1.48	0.06	5.32	0.08	3.84	0.09

Table 1—Continued

ID ^a	X''_{QSO} ^b	Y''_{QSO} ^b	K_{MB} ^c	$R - I$ ^d	error	$R - K$ ^d	error	$I - K$ ^d	error
1029	129.5	-46.9	17.88	0.81	0.03	3.86	0.05	3.05	0.06
1030	350.8	-478.1	17.96	1.08	0.04	4.72	0.04	3.64	0.03
1031	53.6	-130.5	17.97	1.40	0.04	5.15	0.05	3.75	0.05
1032	48.6	-71.9	18.08	0.80	0.04	4.24	0.08	3.44	0.08
1033	224.3	161.0	18.09	1.28	0.07	4.85	0.09	3.57	0.07
1034	44.0	317.5	18.10	0.24	0.03	3.38	0.05	3.14	0.05
1035	31.8	156.8	18.10	0.89	0.06	3.95	0.06	3.06	0.07
1036	317.4	-378.4	18.11	1.11	0.08	4.65	0.07	3.55	0.06
1037	271.7	95.7	18.13	0.58	0.05	2.88	0.07	2.30	0.08
1038	228.4	-445.1	18.13	1.43	0.07	5.02	0.07	3.59	0.06
1039	74.6	-121.3	18.14	0.94	0.02	3.80	0.04	2.86	0.04
1040	371.4	-304.5	18.19	0.48	0.03	2.87	0.17	2.38	0.17
1041	-65.8	289.9	18.30	1.62	0.05	5.73	0.04	4.11	0.05
1042	68.2	-430.9	18.30	1.43	0.08	5.25	0.10	3.82	0.09
1043	135.6	-292.3	18.35	1.30	0.09	5.17	0.18	3.88	0.18
1044	-63.8	-302.6	18.35	1.49	0.24	5.89	0.17	4.41	0.20
1045	62.1	-496.3	18.36	0.82	0.10	4.95	0.07	4.13	0.11
1046	-54.2	-515.5	18.49	1.13	0.20	4.88	0.15	3.75	0.18
1047	-45.5	-255.9	18.50	0.59	0.21	4.37	0.09	3.78	0.21
1048	45.1	-373.1	18.53	1.02	0.09	4.53	0.08	3.52	0.06
1049	251.5	-93.6	18.56	0.43	0.06	3.58	0.10	3.15	0.10
1050	318.1	-72.6	18.57	0.71	0.05	3.73	0.17	3.02	0.17
1051	61.6	6.0	18.58	1.40	0.15	5.43	0.14	4.03	0.08
1052	186.9	51.2	18.61	0.31	0.21	4.63	0.10	4.32	0.22
1053	188.7	-99.6	18.62	0.78	0.18	4.96	0.13	4.18	0.17
1054	-2.9	-178.9	18.70	0.94	0.03	3.88	0.05	2.94	0.06
1055	345.6	98.3	18.75	1.51	0.22	5.37	0.18	3.86	0.21
1056	-38.8	-380.5	18.80	0.81	0.30	4.03	0.46	3.22	0.40

Table 1—Continued

ID ^a	X''_{QSO} ^b	Y''_{QSO} ^b	K_{MB} ^c	$R - I$ ^d	error	$R - K$ ^d	error	$I - K$ ^d	error
1057	230.9	142.7	18.85	1.22	0.04	4.79	0.05	3.57	0.05
1058	372.8	-129.6	18.86	0.91	0.72	5.21	0.52	4.30	0.56
1059	336.2	-269.9	18.86	0.57	0.03	3.14	0.04	2.56	0.05
1060	13.4	258.5	18.87	0.59	0.19	4.52	0.11	3.93	0.20
1061	149.7	310.0	18.90	1.38	0.15	6.16	0.14	4.78	0.10
1062	8.5	-57.8	18.95	1.04	0.07	4.32	0.10	3.28	0.09
1063	-23.8	-404.7	18.96	1.16	0.56	5.22	0.44	4.06	0.48
1064	227.6	-505.7	18.96	0.67	0.05	4.11	0.03	3.44	0.06
1065	146.9	33.3	18.99	0.96	0.13	4.49	0.17	3.53	0.13
2001	734.5	-504.4	14.29	0.92	0.00	3.10	0.00	2.18	0.00
2002	418.9	118.0	14.97	1.20	0.00	3.22	0.00	2.02	0.00
2003	515.1	-345.1	16.13	0.67	0.00	2.40	0.00	1.72	0.00
2004	826.7	123.6	16.29	0.58	0.01	3.39	0.01	2.81	0.02
2005	469.1	148.7	16.46	0.80	0.01	2.61	0.02	1.81	0.02
2006	700.8	202.0	17.10	0.71	0.02	3.41	0.02	2.71	0.03
2007	836.9	-247.3	17.17	0.86	0.01	4.05	0.03	3.19	0.04
2008	424.4	-533.0	17.25	1.61	0.04	5.36	0.03	3.75	0.04
2009	443.5	-72.0	17.37	0.38	0.01	2.48	0.05	2.10	0.05
2010	739.1	398.5	17.37	1.36	0.01	3.46	0.03	2.10	0.03
2011	703.9	406.5	17.44	1.31	0.02	5.19	0.04	3.88	0.04
2012	826.9	-411.6	17.57	0.65	0.06	3.49	0.04	2.85	0.07
2013	576.3	-505.3	17.57	1.49	0.05	5.50	0.04	4.01	0.06
2014	425.9	40.5	17.72	0.71	0.02	3.58	0.04	2.87	0.04
2015	426.4	-251.8	17.85	0.37	0.01	2.45	0.01	2.07	0.02
2016	675.0	434.8	17.92	1.25	0.07	5.40	0.06	4.16	0.06
2017	703.4	256.8	18.31	0.24	0.02	2.62	0.06	2.37	0.06
2018	596.8	177.4	18.67	0.88	0.07	4.08	0.04	3.20	0.07
2019	452.4	-528.7	18.72	1.41	0.16	5.01	0.26	3.59	0.28

Table 1—Continued

ID ^a	X''_{QSO} ^b	Y''_{QSO} ^b	K_{MB} ^c	$R - I$ ^d	error	$R - K$ ^d	error	$I - K$ ^d	error
2020	815.1	76.6	18.78	0.69	0.06	3.32	0.14	2.63	0.15
3001	-552.8	-380.8	16.49	0.65	0.02	3.08	0.02	2.43	0.02
3002	-489.7	-129.1	16.53	0.62	0.01	2.40	0.02	1.78	0.02
3003	-436.1	-347.6	17.04	0.85	0.01	3.49	0.03	2.64	0.03
3004	-473.2	-361.3	17.54	0.79	0.03	4.08	0.06	3.30	0.06
3005	-360.7	-347.5	17.59	0.66	0.01	3.27	0.07	2.61	0.07
3006	-529.8	205.3	17.79	0.27	0.00	1.31	0.07	1.05	0.07
3007	-419.7	309.4	17.93	0.91	0.16	3.66	0.07	2.75	0.16
3008	-523.5	-350.7	17.97	0.45	0.02	2.77	0.03	2.32	0.03
3009	-512.4	101.5	18.04	0.74	0.04	4.06	0.06	3.32	0.06
3010	-232.4	339.8	18.07	0.60	0.02	3.07	0.07	2.46	0.07
3011	-186.7	321.5	18.48	0.71	0.05	3.22	0.04	2.51	0.06
3012	-547.9	217.8	18.52	0.51	0.01	2.73	0.09	2.21	0.09
3013	-420.0	125.1	18.57	0.31	0.03	2.38	0.06	2.07	0.06
3014	-426.1	-517.3	18.62	1.44	0.07	4.66	0.09	3.21	0.09
3015	-286.2	-293.5	18.79	0.81	0.04	3.50	0.04	2.69	0.05
3016	-290.5	338.7	18.93	0.74	0.11	3.43	0.10	2.69	0.15
3017	-246.7	-281.4	18.98	1.53	0.10	5.52	0.05	3.99	0.10
3018	-568.3	12.4	18.99	0.05	0.18	3.10	0.41	3.06	0.45

^aID numbers 1000s, 2000s, and 3000s represent galaxies in the Cluster region, the Western region, and the Eastern region, respectively.

^bRelative offsets for each object from the quasar in arcsec.

^cThe MAG_BEST output for the K -band data produced by SExtractor (Bertin & Arnouts 1996). These values are used as total magnitudes for the galaxies.

^dColors are measured in 3.5-arcsec-diameter apertures for the seeing-matched frames. The tabulated errors are empirical values based on repeated photometry for each object (see Sect. 2).

This figure "hze_fig2.jpg" is available in "jpg" format from:

<http://arxiv.org/ps/astro-ph/9907437v2>